

EASI-STRESS

**EUROPEAN ACTIVITY FOR STANDARDIZATION OF INDUSTRIAL
RESIDUAL STRESS CHARACTERIZATION**

H2020 NMBP-35-2020

Grant Agreement Number: 953219



Deliverable Report:

D4.2 Technical report with mathematical formalisms (equations), dedicated technical drawings and diagrams that describes coordinate systems, variables, workflows for data processing, and that includes the description of the experimental parameters to be included in FE-modelling software

Project Deliverable Information Sheet

EASI-STRESS Project	Project Ref. No. 953219	
	Project Title: EASI-STRESS - European Activity for Standardization of Industrial residual STRESS characterization	
	Project Website: https://easi-stress.eu	
	Deliverable No.: D4.2	
	Deliverable Type: Report	
	Dissemination Level: Public	Contractual Delivery Date: 31/04/2022 Shifted to 31/10/2022
		Actual Delivery Date: 31/10/2022
EC Project Officer: Yanaris Ortega Garcia		

Document Control Sheet

Document	Title: Technical report with mathematical formalisms (equations), dedicated technical drawings and diagrams that describes coordinate systems, variables, workflows for data processing, and that includes the description of the experimental parameters to be included in FE-modelling software	
	Version: 1.0	
	Available at: TEAMS shared site	
	Files: EASI-STRESS_D4.2_FINAL.PDF EASI-STRESS_D4.2_FINAL.DOCX	
Authorship	Written by	Arnold Paecklar Thilo Pirling
	Contributors	Ranggi Ramadan Mohamed Fahres Slim Sandra Cabeza David Canelo Yubero Peter Staron Márton Markó Matthew Roy Veijo Honkimaki Hanna Leemreize Fabien Lefebvre Eric Usmial
	Reviewed by	Nikolaj Zangenberg
	Approved	

List of Figures

Figure 1. Most important features of a diffraction peak. Figure adapted from [11].	10
Figure 2. Representation of the stress tensor in an infinitesimal body.	11
Figure 3. Instrument setup of the X-Raybot.	15
Figure 4. Illustration showing the main measurement axes of laboratory XRD setups.	16
Figure 5. Data analysis workflow for residual stress determination using laboratory X-ray diffractometers.	17
Figure 6. Illustration showing the components, measurement, and instrument axes of the SALSA instrument.	19
Figure 7. Data analysis workflow for residual stress determination using neutron diffraction on SALSA.	19
Figure 8. Illustration showing the components and instrument axes of ATHOS.	20
Figure 9. Data analysis workflow for residual stress determination using neutron diffraction on ATHOS.	21
Figure 10. Schematic showing the components as well as the measurement and instrument axes of the EDD setup at ID15A using a two 1D detector setup.	23
Figure 11. Schematic showing the components as well as the measurement and instrument axes of the ADD setup with a monochromatic beam at ID15A using a 2D detector setup.	23
Figure 12. Data analysis workflow for residual stress determination using energy-dispersive synchrotron X-ray diffraction on ID15A with a 1D detector setup.	24
Figure 13. Schematic showing the components as well as the measurement and instrument axes of the ADD setup with a monochromatic beam at beamline P07 using a 2D detector setup. The setup is used in both hutches EH3 and EH1.	25
Figure 14. Data analysis workflow for residual stress determination using synchrotron X-ray diffraction on P07 beamline.	26
Figure 15. Illustration showing the setup of beamline P61A with the Eulerian cradle nomenclature in the insert (reproduced from [29]).	27
Figure 16. Data analysis workflow for residual stress determination using synchrotron X-ray diffraction on P61A.	27
Figure 17. Summary of the data analysis workflow up to data reduction and data fitting at the participating beamlines.	29
Figure 18. Illustration of data reduction processes to obtain a diffractogram for different types of detectors: (a) 2D PSD detector is integrated over the detector height; (b) Azimuthal angle sectioning followed by radial integration for 2D detector; (c) no integration required for 1D energy-dispersive detector.	30
Figure 19. Diagram showing the common point for harmonisation of data analysis at different instruments proposed by the EASI-STRESS project.	31
Figure 20. Illustration of the first stage of data analysis: raw data is reduced and fitted using instrument-specific data analysis software to produce standardised fitted data output.	32
Figure 21. Proposed data structure of the standardised fitted data output describing the “General_info” group.	34
Figure 22. Proposed data structure of the standardised fitted data output describing the “Point_nnnn” group.	35
Figure 23. Diagrams of the data analysis workflow/algorithm for the common software for residual stress determination.	36
Figure 24. Influence of the positioning error on the final error estimation.	38
Figure 25. Illustration of the strain values at different measurement points.	39

Figure 26. Output format of the calculated stress values in the HDF5 file..... 42

List of Tables

Table 1. LRI instruments in the EASI-STRESS project.	14
Table 2. Main characteristic of the laboratory X-ray devices.	15
Table 3. Mathematical formulation of the common software.	36

List of Abbreviations

AD	Angle-Dispersive
ADD	Angle-Dispersive Diffraction
BCC	Body-Centred Cubic
CHADA	Characterization Data
CSC	Conical Slit Cells
ED	Energy-Dispersive
EDD	Energy-Dispersive Diffraction
FCC	Face-Centred Cubic
FE	Finite Elements
FWHM	Full Width at Half Maximum
GV	Gauge Volume
HCP	Hexagonal Close Packed
LRI	Large-scale Research Infrastructure
NeXus	Neutron, X-ray, (muon) Science
NQL	Neutron Quality Label
TOF	Time-of-Flight
RS	Residual Stress
ROI	Region of Interest
WP	Work Package
XRD	X-ray Diffraction

List of Symbols¹ and units

ε	Elastic strain	-
2θ	Diffraction angle	degrees
ϕ	Orientation angle	degrees
ψ	Orientation angle	degrees
λ	Wavelength	nm
d	Lattice plane spacing	nm
hkl	Family of crystal lattice planes defined by the indices h, k, and l	-
E	Depending on context (photon) energy or Young's modulus	eV/GPa
ν	Poisson's ratio	-
σ_{ij}	Components of stress tensor	MPa
ε_{ij}	Components of the elastic strain tensor	-

¹ All the variables used for the calculations should be treated as being specific for a certain hkl value. For better readability, the notation hkl was omitted in the subsequent equations.

$\alpha, \beta, \gamma, \omega$	Rotation angles	degrees
I	Intensity	counts
Δ	Variation of, or change in, the parameter that follows	-
x, y, z	Axes of the specimen co-ordinate system	-
S_x	Substitution factor for x-direction	-
S_y	Substitution factor for y-direction	-
S_z	Substitution factor for z-direction	-
μ	Lamé constant	Pa
$Tr(\sigma)$	Trace of the stress tensor	-
τ_{ij}	Shear stress components ($i=j$; $i,j=1,2,3$)	MPa
$S_1^{\{hkl\}}, S_2^{\{hkl\}}$	Elasticity constants of the family of lattice planes hkl	-
σ_ϕ	Normal stress value in a direction defined by the angle ϕ	MPa
τ_ϕ	Shear stress value in a direction defined by the angle ϕ	MPa

Subscripts

$\phi\psi$ Indicate the normal component, in the (ϕ) -direction of the quantity concerned
0 (zero) Indicates stress-free value of the quantity concerned

Table of Contents

Project Deliverable Information Sheet	2
Document Control Sheet	2
List of Figures	3
List of Tables	4
List of Abbreviations	4
List of Symbols and units	4
Subscripts	5
Table of Contents	6
Executive summary	8
1. Introduction	9
2. Principles of residual stress determination	9
2.1 Specific equations for neutron and synchrotron radiation based diffraction techniques .	9
2.1.1 Strain	9
2.1.1 Stress	11
2.2 Specific equations for laboratory X-ray radiation	13
2.2.1 Biaxial stress analysis	13
2.2.2 Triaxial stress analysis	13
3. Description of instrument setups, parameters, and current data analysis workflows	14
3.1 Laboratory X-ray Measurements	14
3.2 Neutron Measurements	18
3.2.1 Stress Analyser for Large – Scale engineering Applications (SALSA)	18
3.2.2 ATHOS	20
3.3 Synchrotron X-ray Measurements	22
3.3.1 ID15A	22
3.3.2 P07 - High-Energy Materials Science Beamline (HEMS)	24
3.3.3 P61A - White Beam Engineering Materials Science Beamline (WINE)	26
4. Discussion	28
5. Proposed harmonisation of analysis workflow and comparison with FE modelling	30
5.1 Proposed harmonization of data analysis	30
5.2 Description of the harmonized fitted data input format	31
5.3 Algorithm and mathematical formulation of the common software for residual stress determination	35
5.4 Description of the final residual stress data output format	41
6. Summary and Outlook	42

7. References	43
---------------------	----



Executive summary

The formulation of a harmonised data analysis workflow, a data output structure, and the format for residual stress determination in large-scale research infrastructure instruments is reported. This structure is being used as the foundations for the development of a common software for residual stress analysis, which facilitates the traceability from the experiment (metadata) and data reduction (data) up to the strain/stress analysis (result). This output will further promote an easier exploitation of the measured data for comparison with laboratory X-ray characterization and industrial finite element modelling activities. A detailed description is presented for the different diffraction techniques, including technical drawings and diagrams describing coordinate systems of the equipment used. Original conception of the common software including general structure, variables, workflows for data processing, input data formats, and mathematical formalisms are described. Furthermore, a standardised format for the data output in each stage of the data processing is proposed.

1. Introduction

Residual stress determination can be accomplished through the measurement of elastic lattice strains at the crystalline level using X-ray or neutron radiation. These measurements can be carried out in polycrystalline materials based on their diffraction signal in laboratories (X-ray) and at high-energy synchrotron or neutron facilities. The latter two are considered as Large-scale Research Infrastructure (LRI); all of the above methods have been used for around three decades for internal stress characterization [1-5]. Standards are already available for laboratory X-ray methods as well as neutron methods [6-10]. Despite previous round-robin exercises to demonstrate the feasibility and precision of respective methods, conducted either as part of or supporting the development of guidelines and standards, knowledge residing at LRIs of these techniques has not yet been widely adopted by the industry (or not even known). Additionally, while there is a European standard for laboratory X-ray measurements, there are currently no general stress determination guidelines using synchrotron X-ray radiation, let alone a harmonised guideline which encompasses the different techniques. The project EASI-STRESS aims to address some of these gaps through its work packages (WPs): industrial confidence in the methods is enhanced by validation and benchmarking of neutron, synchrotron X-ray, and laboratory-based techniques with predictive numerical models with benchmark samples in WP2; residual stress determination using different methods at the LRIs are harmonised in terms of measurement protocols and ontologies (WP3), and harmonised metadata and residual stress analysis algorithms in a common software are addressed in WP4. Hence, a setup of industrial service functions for residual stress is initiated through a series of round-robin measurements of industrial cases in WP5. Finally, WP6 aims to produce a technical specification for synchrotron X-ray stress measurements to bring the method closer to a standardized technique.

This document describes the steps which are part of harmonising the data analysis workflows at LRIs. This work serves as the base for the development of a common software for residual stress determination and standardisation of the data output format. General principles of residual stress measurements using neutrons, synchrotron X-ray radiation, and laboratory X-ray radiation are described. This is followed by a brief description of the current state of the instrumental setups, data analysis algorithms, software, and data output format. The presented information was provided by the instrument scientists and researchers involved in WP4. Furthermore, the report describes the proposed data analysis harmonised workflow as well as the description of the data output format and the mathematical formalism. The outlined information is guiding the development of the common software for residual stress determination.

2. Principles of residual stress determination

2.1 Specific equations for neutron and synchrotron radiation based diffraction techniques

2.1.1 Strain

When harnessing diffraction methods for determining residual stress in (poly)crystalline materials, Bragg's law is used:

$$\lambda = 2d \sin \theta \quad (1)$$

which states that the lattice spacing d between parallel crystallographic planes in a crystalline material can be precisely determined by knowing the wavelength λ of the radiation used, and the scattering angle 2θ . While not explicitly pointed out in the subsequent sections, all of the subsequent equations

and its variables correspond to a specific hkl value. Figure 1 illustrates the most important parameters to describe a diffraction peak which include the peak height and intensity, position (Bragg angle 2θ) and full width at half maximum (FWHM).

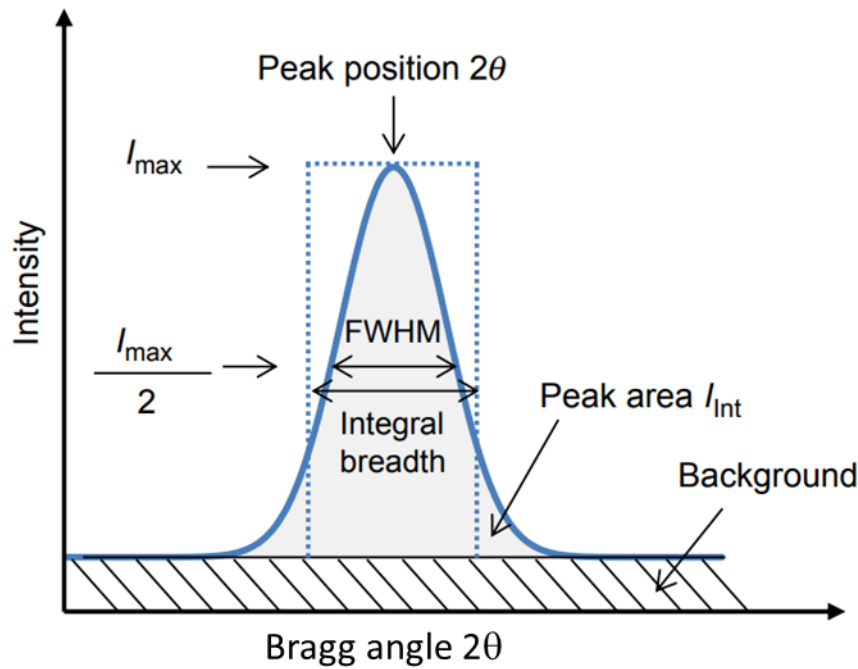


Figure 1. Most important features of a diffraction peak. Figure adapted from [11].

The lattice spacing for a specific crystallographic plane can be used as a strain gauge in a stressed material (externally and/or internally), where the strain ε^2 in the direction of the scattering vector can be calculated as:

$$\varepsilon = \frac{d - d_0}{d_0} \quad (2)$$

where d_0 is the according lattice spacing for the stress-free state of the material, the so called stress-free reference value. In practice, it could be obtained from the same material in which stresses had been minimized as much as possible (such as cutting small coupons and/or applying stress relief heat treatments). The reference could also be taken in a far field point from the stress gradient to compare the intensity of this one vs base material such as in welds. Therefore, this method allows absolute stress values determination. For the angle-dispersive (AD) diffraction method, the change of the lattice spacing is reflected in the shift of the position of the Bragg angle 2θ relative to the one of the reference sample. Inserting Braggs-law (equation 1) in equation 2, hkl specific strain can be determined directly from the measured diffraction angles as follows:

$$\varepsilon = \frac{\sin \theta_0}{\sin \theta} - 1 \quad (3)$$

For Time-of-Flight (TOF) neutron diffraction and energy-dispersive (ED) X-ray diffraction methods, the change of lattice spacing is obtained from the difference in photon energy E or neutron TOF with respect to the reference value E_0 and TOF_0 , respectively. Using the De Broglie equation, which relates a particle's energy to its wavelength, equation (2) can be re-written as:

² In literature strain is sometimes also denoted as e

$$\varepsilon = \frac{E_0}{E} - 1 = \frac{\text{TOF}}{\text{TOF}_0} - 1 \quad (4)$$

where the subscript 0 refers to the stress-free reference material. Generally, neutron TOF diffractometers have two detectors or 2D position sensitive detectors and after data reduction the collected intensity is shown as a function of d . In this case equation 2 can be used. Since neutron TOF measurements give a diffractogram with a larger 2θ range, compared to monochromatic measurements, LeBail-, Pawley-, or Rietveld-refinements can be used to obtain basic lattice parameters with high accuracy. The same is true for synchrotron-radiation measurements where large 2θ ranges can be collected simultaneously. The range can be even increased if the sample-detector distances are reduced.

2.1.1 Stress

In a general three-dimensional case, assuming infinitesimally small deformations, stress and strain can be written in the Cauchy tensor form:

$$\sigma = \begin{bmatrix} \sigma_{xx} & \sigma_{xy} & \sigma_{xz} \\ \sigma_{yx} & \sigma_{yy} & \sigma_{yz} \\ \sigma_{zx} & \sigma_{zy} & \sigma_{zz} \end{bmatrix} \quad (5)$$

$$\varepsilon = \begin{bmatrix} \varepsilon_{xx} & \varepsilon_{xy} & \varepsilon_{xz} \\ \varepsilon_{yx} & \varepsilon_{yy} & \varepsilon_{yz} \\ \varepsilon_{zx} & \varepsilon_{zy} & \varepsilon_{zz} \end{bmatrix} \quad (6)$$

The indices refer to the stress and strain components as shown in Figure 2. The diagonal components of the tensor ($i = j$) represent stresses and strains normal to the surface of the sample, while the off-diagonal components ($i \neq j$) represent shear stresses and shear strains (in-plane).

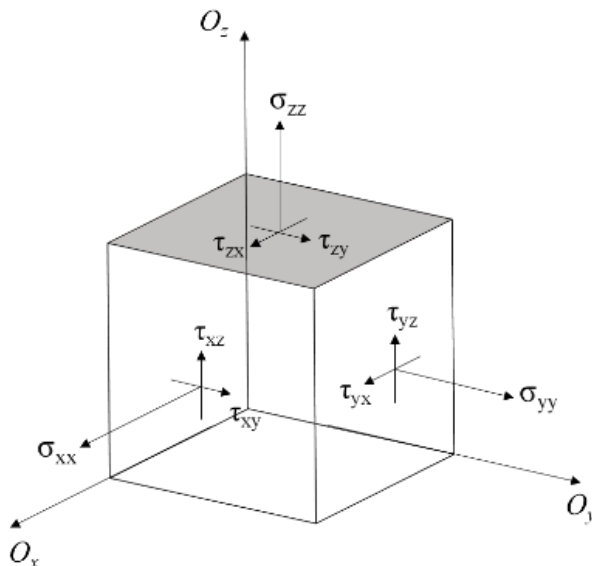


Figure 2. Representation of the stress tensor in an infinitesimal body.

For an elastically isotropic material (equal stiffness in every direction), the stress tensor is symmetric (i.e., $\sigma_{ij} = \sigma_{ji}$). This is also the case for the strain tensor. Therefore, the determination of six components of the stress tensor in a particular point can be achieved by measuring six strain components, given

that the elastic properties of the material are known [1]. The relation between the stress tensor and strain tensor in the elastic regime can be written according to Hooke's law for specific hkl values:

$$\begin{bmatrix} \sigma_{xx} \\ \sigma_{yy} \\ \sigma_{zz} \\ \sigma_{xy} \\ \sigma_{yz} \\ \sigma_{xz} \end{bmatrix} = \frac{E}{(1+\nu)(1-2\nu)} \begin{bmatrix} 1-\nu & \nu & \nu & 0 & 0 & 0 \\ \nu & 1-\nu & \nu & 0 & 0 & 0 \\ \nu & \nu & 1-\nu & 0 & 0 & 0 \\ 0 & 0 & 0 & (1-2\nu)/2 & 0 & 0 \\ 0 & 0 & 0 & 0 & (1-2\nu)/2 & 0 \\ 0 & 0 & 0 & 0 & 0 & (1-2\nu)/2 \end{bmatrix} \begin{bmatrix} \varepsilon_{xx} \\ \varepsilon_{yy} \\ \varepsilon_{zz} \\ 2\varepsilon_{xy} \\ 2\varepsilon_{yz} \\ 2\varepsilon_{xz} \end{bmatrix} \quad (7)$$

where E and ν are the material's Young's modulus and Poisson's ratio, respectively. Neutron diffraction and high-energy synchrotron X-ray diffraction have an advantage over other residual stress measurement methods because they can, in theory, measure the strain in any direction. However, since the principle of strain measurement using diffraction methods is the comparison between interplanar distance of atomic lattice, the diffraction method can only be used to measure directly normal (but not shear) lattice strains.

This problem can be solved by measuring the specific strain components ε_{lmn} in the l , m , and n directions which are the directional cosines with respect to the orthogonal sample coordinate axes O_x , O_y , and O_z . The normal strain ε_{lmn} is related to the six components of the strain tensor like this:

$$\varepsilon_{lmn} = l^2 \varepsilon_{xx} + m^2 \varepsilon_{yy} + n^2 \varepsilon_{zz} + 2lm\varepsilon_{xy} + 2mn\varepsilon_{yz} + 2ln\varepsilon_{xz} \quad (8)$$

The measurement of the normal strain components $\varepsilon(l_f, m_f, n_f)$ in six ($f = 1, \dots, 6$) or more different directions leads to a system of linear equations with six unknown components of the strain tensor which can be written as:

$$\begin{bmatrix} \sigma(l_1, m_1, n_1) \\ \sigma(l_2, m_2, n_2) \\ \sigma(l_3, m_3, n_3) \\ \sigma(l_4, m_4, n_4) \\ \sigma(l_5, m_5, n_5) \\ \sigma(l_6, m_6, n_6) \\ \vdots \\ \sigma(l_f, m_f, n_f) \end{bmatrix} = \begin{bmatrix} l_1^2 & m_1^2 & n_1^2 & 2l_1m_1 & 2m_1n_1 & 2l_1n_1 \\ l_2^2 & m_2^2 & n_2^2 & 2l_2m_2 & 2m_2n_2 & 2l_2n_2 \\ l_3^2 & m_3^2 & n_3^2 & 2l_3m_3 & 2m_3n_3 & 2l_3n_3 \\ l_4^2 & m_4^2 & n_4^2 & 2l_4m_4 & 2m_4n_4 & 2l_4n_4 \\ l_5^2 & m_5^2 & n_5^2 & 2l_5m_5 & 2m_5n_5 & 2l_5n_5 \\ l_6^2 & m_6^2 & n_6^2 & 2l_6m_6 & 2m_6n_6 & 2l_6n_6 \\ \vdots & \vdots & \vdots & \vdots & \vdots & \vdots \\ l_f^2 & m_f^2 & n_f^2 & 2l_fm_f & 2m_fn_f & 2l_fn_f \end{bmatrix} \cdot \begin{bmatrix} \varepsilon_{xx} \\ \varepsilon_{yy} \\ \varepsilon_{zz} \\ \varepsilon_{xy} \\ \varepsilon_{yz} \\ \varepsilon_{xz} \end{bmatrix} \quad (9)$$

A careful selection of directions (l_f, m_f, n_f) , which provide linearly independent strain components, is required to ensure the accuracy of the stress tensor determination. The measurement of more than 6 strain components ε_{lmn} creates an overdetermined system from equation (9), and the strain tensor can be solved by the least-squares method. From this strain tensor determination, the stress tensor can be calculated using equation (7).

The choice of measuring directions is mostly constrained by material or experimental restrictions [12]. A material's properties such as coarse grain size and/or texture and, on the other hand, limited beam time in the case of neutron and synchrotron facilities force the experimenter to optimize the number of orientations and/or points. Therefore, the characterization and resolution of strain gradients in the sample is adapted to only critical regions and/or directions before the experiment. For these reasons, mostly three orthogonal strain components are measured to determine the corresponding three orthogonal stress components for a specific hkl (equation 10).

$$\sigma_{xx} = \frac{E}{(1+\nu)(1-2\nu)} [(1-\nu)\varepsilon_{xx} + \nu(\varepsilon_{yy} + \varepsilon_{zz})] \quad (10)$$

$$\sigma_{yy} = \frac{E}{(1+\nu)(1-2\nu)} [(1-\nu)\varepsilon_{yy} + \nu(\varepsilon_{xx} + \varepsilon_{zz})]$$

$$\sigma_{zz} = \frac{E}{(1+\nu)(1-2\nu)} [(1-\nu)\varepsilon_{zz} + \nu(\varepsilon_{xx} + \varepsilon_{yy})]$$

2.2 Specific equations for laboratory X-ray radiation

The equation for expressing the strain in the direction defined by the angle ψ (Psi) and ϕ (Phi) in its general form is as follows:

$$\varepsilon_{\phi\psi}^{\{hkl\}} = S_1^{\{hkl\}}[\sigma_{11} + \sigma_{22} + \sigma_{33}] + \frac{1}{2}S_2^{\{hkl\}}\sigma_{33}\cos^2\psi + \frac{1}{2}S_2^{\{hkl\}}[\sigma_{11}\cos^2\phi + \sigma_{22}\sin^2\phi + \tau_{12}\sin 2\phi]\sin^2\psi + \frac{1}{2}S_2^{\{hkl\}}[\tau_{13}\cos\phi + \tau_{23}\sin\phi]\sin^2\psi \quad (11)$$

Where $S_1^{\{hkl\}}$ and $S_2^{\{hkl\}}$ are the X-ray elastic constants for the family of lattice planes $\{hkl\}$ further defined as:

$$S_1^{\{hkl\}} = \left(-\frac{\nu}{E}\right)_{hkl} \quad \text{and} \quad S_2^{\{hkl\}} = \left(\frac{1+\nu}{E}\right)_{hkl}$$

σ_{11} , σ_{22} , and σ_{33} are the normal stress components in the directions S_1 , S_2 , and S_3 , and τ_{12} , τ_{13} , τ_{23} are the shear stresses within the plane defined by S_1 and S_2 , S_1 and S_3 , and S_2 and S_3 , respectively. In most materials the penetration depth of X-rays is in the order of tens of micrometres. Therefore, it can often be assumed that $\sigma_{33} = 0$, which simplifies equation (11) to

$$\varepsilon_{\phi\psi}^{\{hkl\}} = S_1^{\{hkl\}}[\sigma_{11} + \sigma_{22}] + \frac{1}{2}S_2^{\{hkl\}}[\sigma_{11}\cos^2\phi + \sigma_{22}\sin^2\phi + \tau_{12}\sin 2\phi]\sin^2\psi + \frac{1}{2}S_2^{\{hkl\}}[\tau_{13}\cos\phi + \tau_{23}\sin\phi]\sin^2\psi \quad (12)$$

2.2.1 Biaxial stress analysis

$\varepsilon_{\phi\psi}^{\{hkl\}}$ are obtained for different combinations of ψ and ϕ angles from experimental measurements. If the stress in the material is biaxial ($\tau_{13} = \tau_{23} = \sigma_{33} = 0$), then, based on equation (12), it can be deduced that the dependence of $\varepsilon_{\phi\psi}^{\{hkl\}}$ on $\sin^2\psi$ is linear.

$$\varepsilon_{\phi\psi}^{\{hkl\}} = \frac{1}{2}S_2^{\{hkl\}} \cdot \sigma_{\phi} \sin^2\psi + S_1^{\{hkl\}} \cdot Tr(\sigma) \quad (13)$$

where: $Tr(\sigma) = (\sigma_{11} + \sigma_{22})$

Plotting $\varepsilon_{\phi\psi}^{\{hkl\}}$ vs. $\sin^2\psi$ for the biaxial case yields then a straight line. For a specific ϕ value, the corresponding σ_{ϕ} value can be obtained by calculating the slope of the straight line.

2.2.2 Triaxial stress analysis

As most laboratory-based (low-energy) X-ray set-ups are only able to assess biaxial stress states, this section commonly applies to laboratory instruments with high energy X-ray sources (i.e. rotating- or liquid-anode), synchrotron X-ray beamlines, or neutron sources. If there are shear stresses present in the planes perpendicular to the sample surface ($\tau_{13} \neq 0$ and /or $\tau_{23} \neq 0$) then the plot of $\varepsilon_{\phi\psi}^{\{hkl\}}$ vs.

$\sin^2 \psi$ is elliptical with a ψ -splitting at $\psi=0$. In addition, if σ_{33} is not equal to zero, then the slope of the $\sin^2 \psi$ plot is proportional to $\sigma_\phi - \sigma_{33}$. This changes equation (13) to the following

$$\varepsilon_{\phi\psi}^{\{hkl\}} = \frac{1}{2} S_2^{\{hkl\}} \cdot (\sigma_\phi - \sigma_{33}) \sin^2 \psi + \frac{1}{2} S_2^{\{hkl\}} \cdot \tau_\phi \sin 2\psi + \frac{1}{2} S_2^{\{hkl\}} \cdot \sigma_{33} + S_1^{\{hkl\}} \cdot Tr(\sigma) \quad (14)$$

where: $Tr(\sigma) = (\sigma_{11} + \sigma_{22} + \sigma_{33})$

At a specific angle ϕ , the values for σ_ϕ and τ_ϕ can be obtained by least square fitting of the strain data using equation (14). Subsequently, the stress tensor can be derived by measuring three different ϕ angles at a minimum of three different ψ angles.

3. Description of instrument setups, parameters, and current data analysis workflows

This section briefly describes a selection of neutron, synchrotron, and laboratory X-ray instruments used for residual stress measurements. The LRI instruments involved in the EASI-STRESS project are:

Table 1. LRI instruments in the EASI-STRESS project.

Institution	Instrument	Type	Country	Website
ILL	SALSA	Neutron AD	France	https://www.ill.eu/users/instruments/instruments-list/salsa/description/instrument-layout
ESRF	ID15A	Synchrotron ED	France	https://www.esrf.fr/home/UsersAndScience/Experiments/StructMaterials/ID15A.html
PETRA III	P07	Synchrotron AD	Germany	https://photon-science.desy.de/facilities/petra_iii/beamlines/p07_high_energy_materials_science/index_eng.html
PETRA III	P61A	Synchrotron ED	Germany	https://photon-science.desy.de/facilities/petra_iii/beamlines/p61_high_energy_wiggler_beamline_lvp/p61a_white_beam_engineering_materials_science_hzg/index_eng.html
BNC	ATHOS	Neutron AD	Hungary	https://www.bnc.hu/?q=athos

Within the EASI-STRESS project, laboratory X-ray measurements are performed at CETIM, DTI, EDF, Siemens Camessa, and the University of Manchester. The descriptions below comprise the instruments' main components, parameters, and data analysis workflows currently available.

3.1 Laboratory X-ray measurements

Laboratory X-ray diffraction measurements are normally carried out using the angular dispersive method with diffractometers which are usually commercially produced. These systems are provided by many different companies which included, but are not limited to, Bruker, PANalytical, PROTO, stresstech, Pulstec, and MRXrays.

The instrumental setup and equipment specifically used by the EASI-STRESS partners is described in detail below:

- **CETIM**
Three X-Raybots from MRX-rays
- **DTI**
X-Raybot from MRX-rays

- **UoM**
PROTO
- **EDF**
X-Raybot from MRX-rays
PROTO
- **Siemens Camessa**
 μ -X360s Portable X-ray Residual Stress Analyzer from Pulstec

Table 2 presents the main characteristics of the three instruments used in the EASI-STRESS project as the tension, current, Psi angles or configurations, etc... The available angle and wavelength allow to study peaks with high multiplicity (e.g. for the alloy 600, crystallographic plan study is (311) with Mn tube => 157.51° 2 θ .) Figure 3 shows an instrumental setup of the X-Raybot.

Table 2. Main characteristic of the laboratory X-ray devices.

Instrument	Tension (kV)	Current (mA)	Angular range of detector ($^{\circ}2\theta$)	Psi angle range ($^{\circ}$)	Portable	Available wave length (K_{α})	2 θ available	Positioning	Configuration
X-raybot	25 ³	1	~25	-40 to 40	yes	Cr, Mn, Cu	140 to 156	By contact or laser	Psi or Omega
Proto	25	20	10	-35 to 35	yes	Cr, Mn	79° - 160°	By contact	Omega
μ -X360s	30	1,5			yes	Cr, Cu, Co, Mn.		By laser	Cos α

Usually, before each analysis or at least once a month if no change of tube occurs during the month, a powder of the alloy of the part is measured in order to check the measurement device (verification that the powder is at zero residual stresses) and a standard reference sample in compression (produced by shot pining) representative of the alloy studied to verify the parameters and measurement chain.

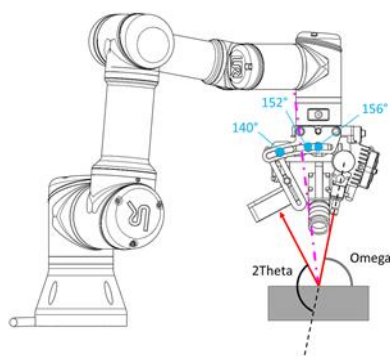


Figure 3. Instrumental setup of the X-Raybot.

General description of laboratory X-ray measurements:

Residual stress measurements using laboratory X-ray sources are usually done using either the $\sin^2(\psi)$ method or the newer $\cos(\alpha)$ method. The most commonly used is the $\sin^2(\psi)$ method, which will be in the focus here. In the $\cos(\alpha)$ method, a 2D detector is used to get the entire Debye-Scherrer

³ This represents the maximum value. The recommended tension is 20 kV.

ring in one single exposure from which both, normal and shear stresses can be extracted, eliminating the need for the psi-tilts. The method is hence faster than the $\sin^2(\psi)$ method. More details about the latter technique can be found in [13].

The instruments using the $\sin^2(\psi)$ method fall into two categories where either the sample is static with the source and detector moving to the different psi angles, or the reverse where the source and detector are static, and the sample is tilted to reach the different psi tilts. The latter can be done using a conventional powder diffractometer where the sample can be tilted, while the first requires specialised setups. There are different instrument configurations working with 0D, 1D, and 2D detectors.

The measurement techniques done on these laboratory X-ray systems follow the EN 15305:2009 standard: *Test methods for residual stress analyses by X-ray diffraction*. The choice of X-ray tube and filter is dictated by the material to be characterised and the analysis parameters will be adapted according to the diffraction properties of the material and geometry of the analysed area. The method tracks the shift in 2θ of a single peak as the diffraction vector is tilted away from the surface normal. The measured stress direction is parallel to the psi tilt direction.

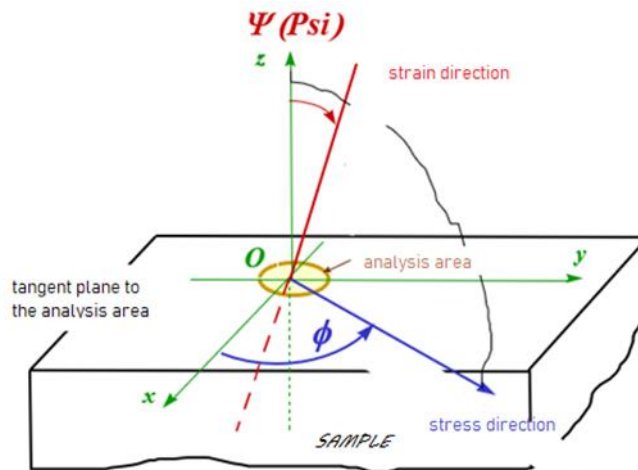


Figure 4. Illustration showing the main measurement axes of laboratory XRD setups.

Measurements are taken at equal steps of, for instance, 0.05 in $\sin^2(\psi)$ from -0.5 to +0.5 ($\pm 45^\circ$ in psi), at $\phi = 0^\circ, 45^\circ$, and 90° . The so obtained diffractogram (counts vs. 2θ angle) show a single diffraction peak for each measurement taken at a given psi angle. Typically, around 10-20 angles are collected and fitted according to equation 13. The gauge volume depends on the penetration depth, which is given by the wavelength of the used X-ray source and the material being probed (and to a smaller degree the incident psi angle), but is estimated to be on average $5 \mu m$. It has to be noted that both the area and depth probed changes during the measurement when the psi angle is changed. Therefore, we are actually not measuring the same volume during the entire measurement consisting of a tilt series. Typical beam sizes on the sample are in the range of 0.4 – 4 mm. The beam size is determined by the collimators. The available collimators for the X-Raybot are 0.5, 1, and 2 mm. The PROTO instrument does not only have different sizes (0.5, 1, 2, and 4 mm) but also in addition to cylindrical collimator rectangular collimators. Since the beam is divergent, the size of the beam on the sample cannot be directly based on the collimator beam size. For example, DTI has collimators with a diameter between 0.5 and 2 mm, but due to the sample to detector distance of approximately 125 mm, there is a divergence after the collimator which increases the beam size on the sample by an estimated 1 mm. Similarly, the multiplication factor applied at EDF is roughly 1.5. Hence, if the

collimator size is 2 mm, the spot on the sample will be 3 mm. Another variable that needs to be considered is the incident angle of the radiation. If the beam is perpendicular to the surface of the sample, its shape is circular, but becomes distorted or even ellipsoidal upon variations of the incident ψ angle. The positioning of the gauge volume can be done manually or by using a laser profilometer which can achieve a precision up to 6 μm .

A general data analysis workflow for residual stress determination using laboratory X-ray diffractometers is illustrated in Figure 5.

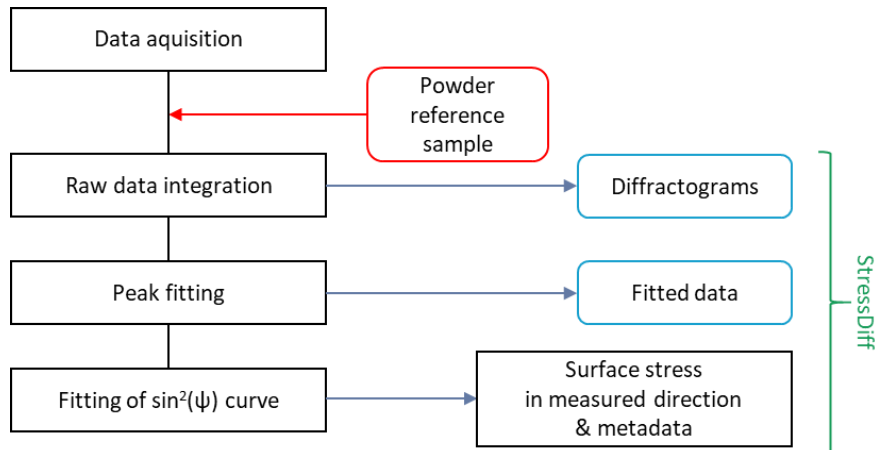


Figure 5. Data analysis workflow for residual stress determination using laboratory X-ray diffractometers.

The software packages and data format used depends on the provider of the system. For instance, the raw data from scans done by the X-raybot are saved in the **.uxd** or **.raw** format. While MRX's software (called StressDiff) processes these files and gives a list with position and stress with associated errors, peak widths and other fitting parameters, it can equally be processed by a lot of other commercially available software packages. Other providers like Bruker use either Topaz or DIFFRAC.LEPTOS or some PANalytical systems use Stress Plus. At CETIM, the standard software package is StressDiff, but for more complicated materials involving difficulties during the peak fitting procedure, open-source software package such as X-light [14], and MAUD (Material Analysis Using Diffraction) [15,16] are used and have already provided agreeable results. With the aforementioned software, background determination and fitting of the diffraction peaks is done as well as the stress determination. The fitted peak positions (peak center, maximum,...) for the diffraction angle, 2θ , can then be plotted versus $\sin^2(\psi)$. The slope of the plot of these data is being used to calculate the normal and shear stress for a specific hkl value, as outlined under section 2.2. The error calculation depends on the software package that is being used. For example, in the standard exported format from the MRXrays X-Raybot, two error values are provided:

I_{stat.}: Statistical error bar. It is deduced from the uncertainties of the peak treatment results.

I_{régr.}: Global error bar deduced from least squares fitting residue.

In the first (statistical), only the fitting error from the peak fitting is used. In the second (global), the fitting error from the $\sin^2(\psi)$ fit is also included. However, these uncertainties should not be confused with the measurement uncertainty as defined in the ISO standard 98-3:2008 "Guide to the Expression of Uncertainty in Measurement" (GUM) [17] and in the national guides for good measurement practice [6]. An in depth description of the evaluation of uncertainties for laboratory X-ray measurements (including numerical examples) can be found in Appendix 1 of [6].

3.2 Neutron Measurements

3.2.1 Stress Analyser for Large – Scale engineering Applications (SALSA)

SALSA is a monochromatic neutron stress diffractometer located at the Institut Max von Laue - Paul Langevin (ILL), Grenoble, France. The schematic of SALSA is shown in Figure 6. The neutron beam on SALSA is monochromated to a narrow incident wavelength distribution using an arrangement of silicon single crystals, cut in the Si(400) direction. The monochromator provides vertical focalization of the 200 mm high incoming beam to a 20 mm focus at the sample position. Horizontal variable curvature of the crystals allows optimization of angular resolution. Additionally to the Si(400) reflection, Si(311), Si(422) and Si(511) are accessible thus providing a wavelength-range between 1.3 and 2.4 Å.

The gauge volume (GV) is defined by three radially focusing collimators, mounted in series: two collimators (col1 and col2, see fig. 6) in the primary beam define horizontal and vertical incoming beam dimensions, a third collimator (col3) between sample and detector defines the remaining horizontal dimension of the diffracted beam. The following beam widths are available: 0.6, 2 and 4 mm for the horizontal and 0.6, 2, 4, 10, 20 mm for the vertical dimension. The distance between gauge volume and collimators ranges from 150 mm for high resolution to 411 mm for large gauge volumes, thus leaving a considerable space for sample manipulations. The GV is selected according to the microstructure and the residual strain gradient to resolve, accounting as well for the compromise of acquisition times and absorption (region of interest vs beam path).

The sample stage is a hexapod or Stewart platform, a parallel kinematics robotic device with 6 degrees of freedom for translation (Tx, Ty, Tz) and rotation (Rx, Ry, Rz) movements. The maximum range is ± 300 mm in translation and $\pm 30^\circ$ in rotation. To extend the tilt range an Eulerian Cradle can be mounted on top of the sample table. The hexapod is linked to the 360° ω -rotation of the instrument and can be displaced horizontally for hosting large samples by 700 mm on the radius of ω . The maximum load capacity is 1000 kg and samples with dimensions up to a couple of meters can be mounted. The positioning accuracy lies below 5 μm . The hexapod control allows the adaptation of the working coordinate system to the sample coordinate system. It is therefore possible to pilot a measurement directly in sample coordinates, store them in meta-data and thus avoiding the necessity of coordinate transformation prior to data analysis.

SALSA's detector is a position sensitive ^3He gas-filled proportional neutron detector. Position sensitivity is achieved through a 2-D grid of 2×128 wires. Through interpolation, the number of channels is extended to 256×256 . This leads to an average pixel size of 0.044° at a distance of 1250 mm from the centre of the instrument. It covers a range of $\sim 11^\circ$. The detector position can be changed between 0° and 135° according to the material under investigation and the net-plane hkl targeted. A more comprehensive description of the instruments can be found elsewhere [18].

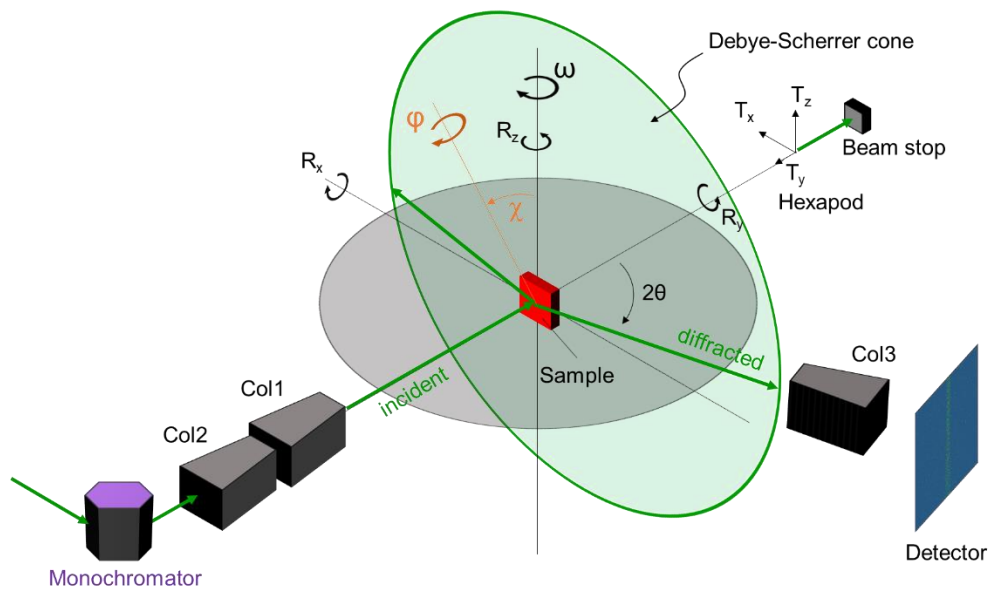


Figure 6. Illustration showing the components, measurement, and instrument axes of the SALSA instrument.

The flowchart in Figure 7 describes SALSA's data analysis workflow. Raw data including metadata are saved in NeXus format [19], and the raw data reduction (calibration, integration...peak fitting) is performed using an in-house data analysis routine called LAMP (Large Array Manipulation Program) [20] that will soon be replaced by another software package called Mantid [21]. The raw data integration is performed by integrating the neutron counts over the detector height, while a calibration routine converts the detector channels into the angular position 2θ using a look-up table generated from a separate calibration measurement. The data reduction routine produces a diffractogram showing the Bragg peaks appearing in the selected angular region. Bragg peaks are then fitted using an analytical model describing the peak shape (e.g., Gaussian, Lorentzian, or Pseudo-Voigt). The fitting results are then compiled together, including selected metadata (T_x , T_y , T_z , ω , detector position...) plus an extra complete instrument metadata file, saved in a regular ASCII text file format. After the transition to Mantid these data will be stored in the NeXus-Stress format, implemented for the EASI-STRESS project between neutron and synchrotron partners.

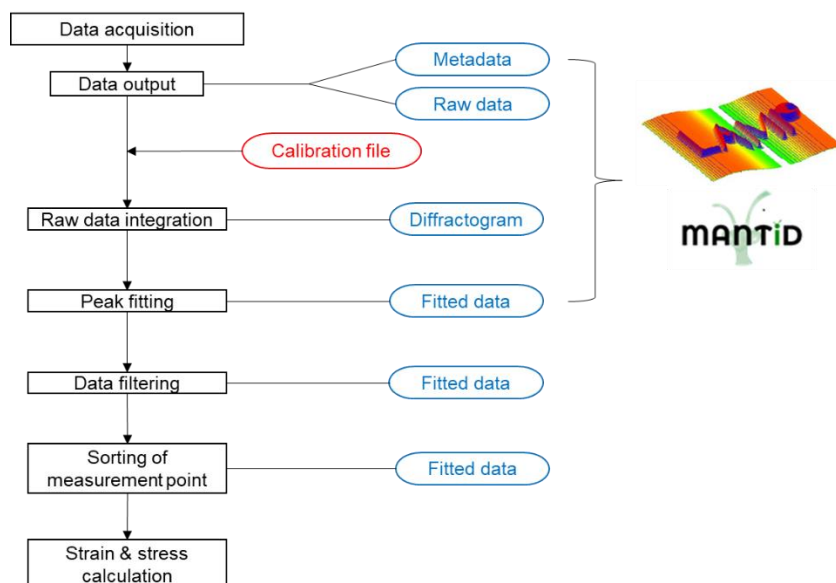


Figure 7. Data analysis workflow for residual stress determination using neutron diffraction on SALSA.

The next step is to filter the peak fitting results by examination of the fitted curves and/or inspection of the fitting parameters (i.e., peak height, width, etc.) and their uncertainties. The quality of the fit is influenced by the measurement conditions under which data were collected. Difficulties and higher levels of error in fitting could be based on factors such as insufficient counts, partially-filled gauge volume, large grains compared to the gauge volume etc., which have been documented extensively in literature [22-26]. The influence of some of these factors on the final stress values can be corrected with specific algorithms. The in-house developed program PS-Fit is used for correcting pseudo strain affected data, specifically for near surface/interface stress determination.

The measurement positions are then sorted, transferred into sample coordinates and interpolated. Using the result from the d_0 -reference measurement, performed at the exact same experimental set-up, strains and stresses are calculated as outlined in equations 3, 7 or 10.

3.2.2 ATHOS

ATHOS is a monochromatic neutron diffractometer at the Budapest Neutron Center (BNC) optimised for residual stress analysis of engineering components. The schematic of ATHOS is shown in Figure 8, followed by a brief description of the main components.

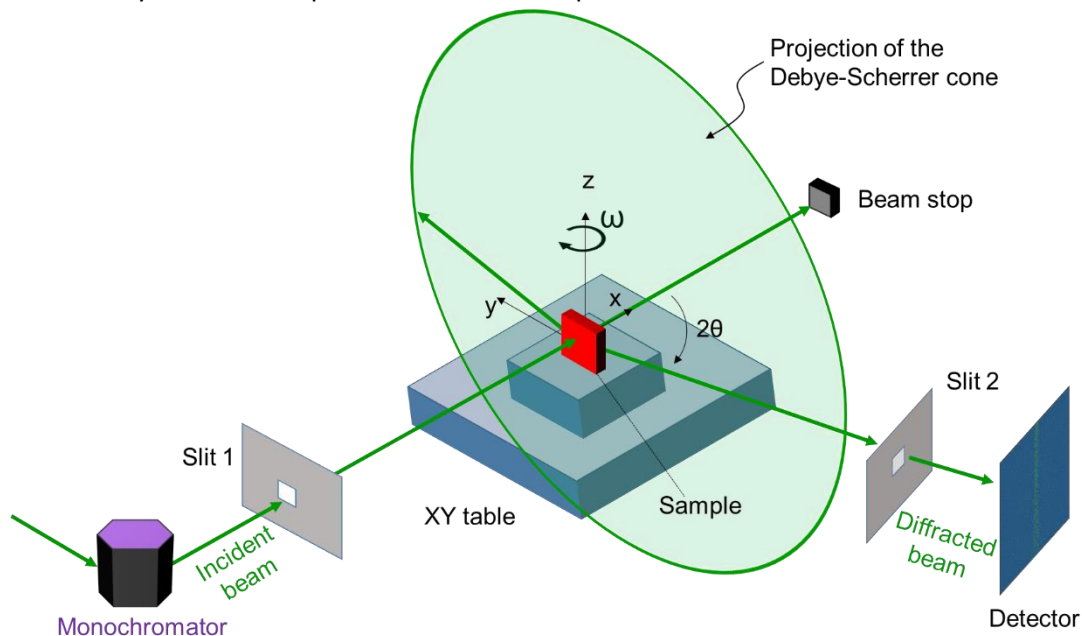


Figure 8. Illustration showing the components and instrument axes of ATHOS.

The neutron beam is monochromatic with an arrangement of pyrolytic graphite single crystals to select the incident wavelength used in the instrument. This monochromator is a vertically-focusing type with pyrolytic graphite crystals. It has a variable radius of curvature, orientation, and tilt to optimise the incident beam according to the specimen to cover a range of wavelengths from 2 - 6 Å, and 1 - 3 Å using the second order reflection. There are three different table options for mounting the sample. A XY table can move the sample in two horizontal directions. The Omega table allows to rotate the sample around the vertical axis. A XZ table functions as an alternative to the XY table and allows to move the sample in a vertical plane. There is a pre-sample collimator, the beam optics, which regulates the vertical and horizontal dimension of the incident beam. The after sample collimator is the beam optics which regulates the vertical and horizontal dimension of the diffracted beam. It is mounted on the detector shielding. The detector at ATHOS comprises a 2-D delay-line type ^3He PSD

with an active area of $180 \times 180 \text{ mm}^2$, covering $\sim 12^\circ$ in 2θ at a distance of 900 mm from the sample. The resolution is 1.6 mm. The data are stored in a 1024×1024 matrix.

A flowchart describing ATHOS's data analysis workflow is provided in Figure 9. The black boxes connected by vertical arrows describe sequential stages of the data analysis workflow. Each box is connected to a blue rounded box indicating the output of the analysis stage. The rounded box connected by a horizontal red arrow to the analysis workflow are input which originated from calibration measurements, which are separated from the main experiment.

On ATHOS, the data analysis workflow up to the peak fitting stages is handled using the Zsamo software developed at BNC and written in Python. A detailed description regarding each stage is provided below. Here, the "refinement of positioning" and "pseudo-strain correction" steps are not described.

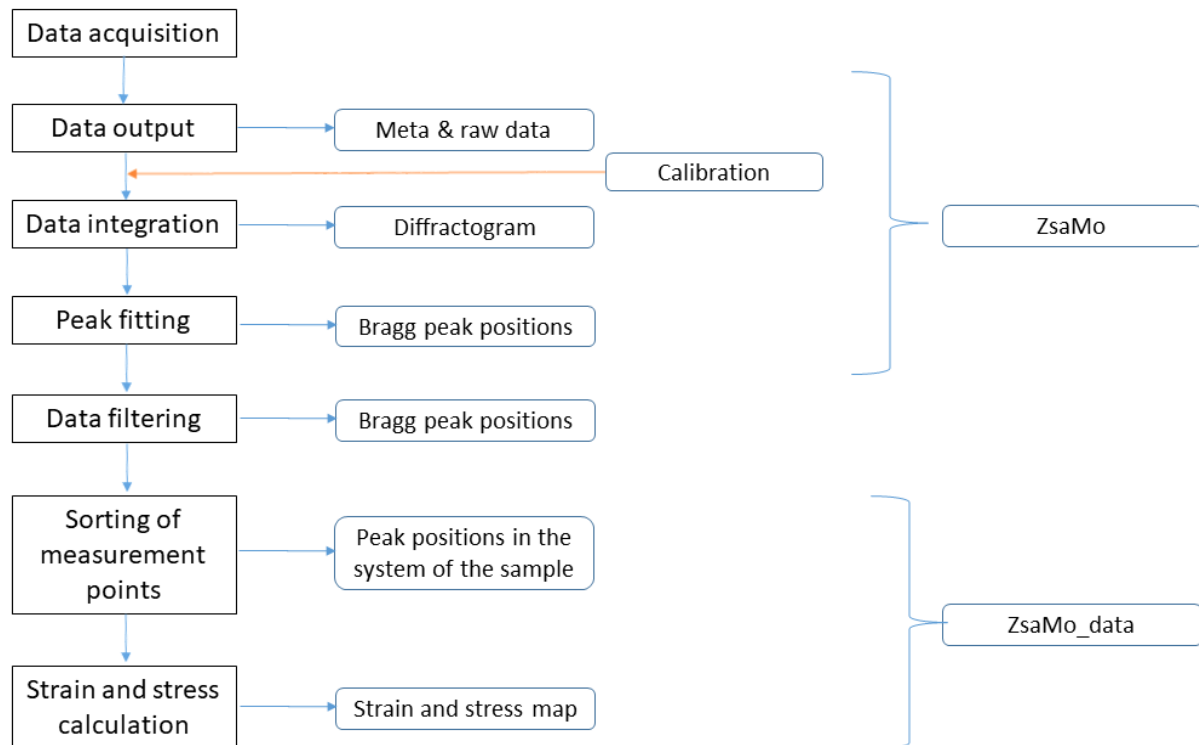


Figure 9. Data analysis workflow for residual stress determination using neutron diffraction on ATHOS.

For the raw data acquisition, each measurement is programmed (single point: cnt, scanning in one motor angle: scan, scanning in one line from a specified position of 2D table at a given direction). Each measurement point is saved under a unique run number. Stress determination on each point requires at least three separate measurements and thus three separate run numbers and files.

For the raw data output on ATHOS, the count data is saved in two formats: TDC and CSV. The TDC format is the native format of the TDC card of the detector. The raw data matrix with the motor position is saved by the Zsamo program in a serialized Python data file. The program also performs the basic data reduction. The transformation of the serialized file to a NeXus file is currently under development. Each measurement point is stored in a different file and the result of the scan and different scans are merged at the later data treatment steps.

The next step is to obtain a diffractogram from the raw data. This is done by integrating the neutron counts over the height of the detector. The correction for curving of the Debye-Scherrer ring and the tilt angle of the detector can be done by using a different data reduction script which is currently being

tested. The two data reduction methods give the same center position and differ only in the width of the fitted Gaussian function even if the scattering angle of the sample is 78° . Each data set represents a detector channel, i.e. channel number 0 - 1023. First, the Zsamo program integrates this data into a 256×256 matrix to decrease the problem with error calculation (i.e. at low counts the Poisson distribution differs highly from the Gaussian one). With this matrix size the number of pixels in the active area are close to that the number of wires in the detector.

During the raw data reduction step, Zsamo does not convert the pixel number to a scattering angle. Subsequent calculations are done with the scattering angle differences. The calibration measurement produces a lookup table which provides the relationship between the position change in the detector and the angular difference between each of two channels, $\Delta 2\theta(i,j)$.

Once the diffractogram is obtained, the next step is to accurately determine the Bragg peak position by fitting the peak profile using an appropriate model. The default fitting routine fits a Gaussian function on the whole reduced data, then fits again the peak within the region of interest (ROI) which is centered at the peak position and has the width of two FWHM where the center and the FWHM value is the result of the first fit. There is an option to skip the second fit as well as changing the size of the ROI in the second fit. The fitting results (peak height, position, FWHM, fitting uncertainties, etc.) are then compiled together with the measurement metadata and the instrument metadata (e.g., omega, 2theta), and reported as the fitted data in a regular Python list. The next step is to evaluate the fitting result, by visual examination of the fitted curve and/or inspecting the fitting parameters (i.e., peak height, width, etc.) and its uncertainties. In the fitted data output, the fitting parameters are saved as a function of the measurement position in the instrument coordinate system. Presently, the transformation from the instrument metadata to the coordinates in the sample's coordinate system is done manually (using different scripts outside the Zsamo package). The lattice strain ϵ_{hkl} is calculated from the fitted 2θ position of the measured points and the stress-free/reference value using equation (3). Subsequently, stresses are then calculated for each point using Hooke's law (equation 10). Codes written in Mathcad and in Python are available on ATHOS to facilitate the data analysis stage from data filtering to strain and stress calculation.

Currently, there is no automatic process in place that writes the processed data according to the NXstress format into a NeXus file. A first example for a data sets measured with ATHOS was converted manually.

3.3 Synchrotron X-ray Measurements

3.3.1 ID15A

ID15A is a beamline at ESRF dedicated to applications of high energy X-ray radiation to materials chemistry and engineering. The materials engineering end-station is dedicated for strain/stress mapping in the bulk of thick components. There are two available setups: an energy-dispersive diffraction (EDD) set-up and an angle-dispersive diffraction (ADD) set-up. Based on what method is selected, different detector and optics setups are to be used. EDD uses two 1D solid state detectors with a white beam while ADD use a 2D area detector with a monochromatic beam. The EDD and ADD setups are shown in Figure 10 and Figure 11, respectively. In the EDD the incident white beam is shaped horizontally and vertically by the set of beam slits. The instrument is equipped with a sample stage providing three translations (T_x , T_y , and T_z) and two rotations (R_y and R_z). An Eulerian cradle, equipped with a translation stage, is mounted on the rotation stage. This allows to precisely orientate the sample around the beam and to probe different directions. The two Germanium solid state

detectors are used to measure the diffraction patterns as a function of the energy. These two detectors are fixed to a diffraction angle $2\theta = 5^\circ$ in both horizontal and vertical directions of the Debye-Scherrer ring. Therefore, diffractograms are acquired in the two orthogonal directions at the same time, allowing for two strain components being measured at the same time. Front and back slits are used to define a gauge volume in the sample for each detector.

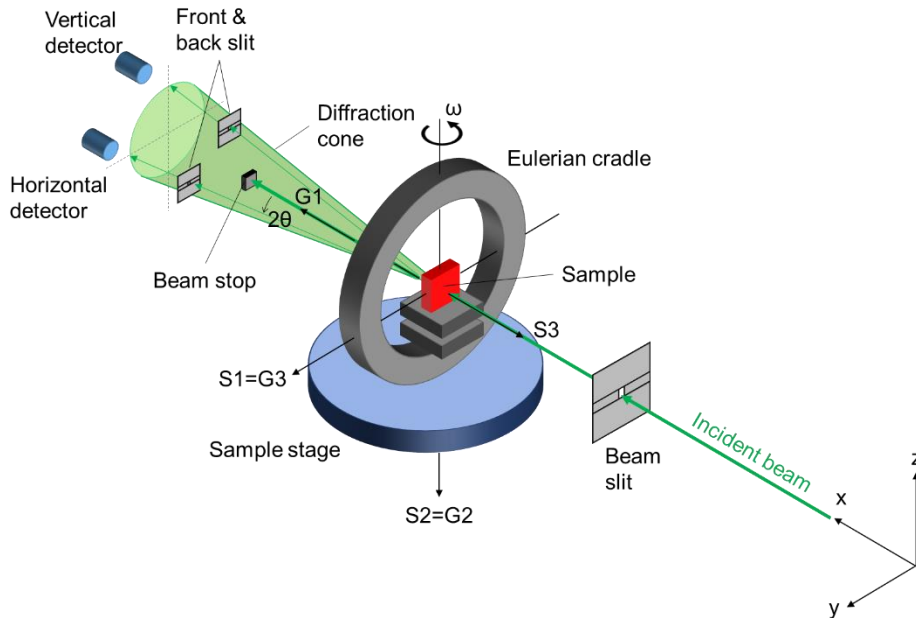


Figure 10. Schematic showing the components as well as the measurement and instrument axes of the EDD setup at ID15A using a two 1D detector setup.

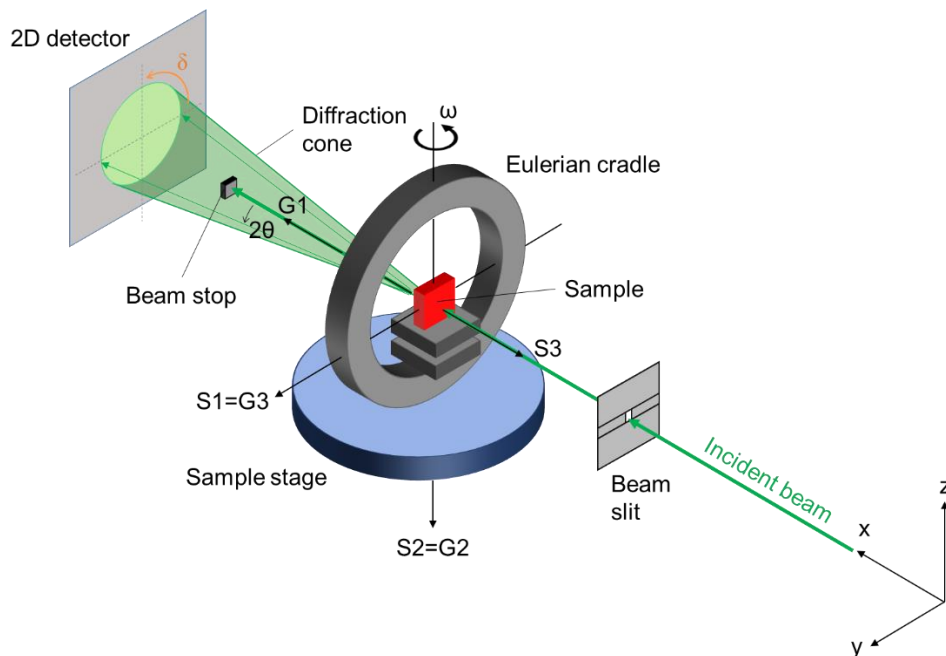


Figure 11. Schematic showing the components as well as the measurement and instrument axes of the ADD setup with a monochromatic beam at ID15A using a 2D detector setup.

A flowchart describing the data analysis workflow of the EDD setup on ID15A is presented in Figure 12. The boxes present the different tasks of the workflow. At each task a NeXus file containing the results is generated. All the steps are executed automatically using Python scripts which were

developed during the EASI-STRESS project. The raw data are written in a NeXus file which can contain multiple scans of different types (e.g. point scan, line scan). At different times during the experiments, the fluorescence lines of a known radioactive source, usually Ba, are acquired. These lines are used for the energy calibration allowing the conversion of channels into energy. The function used for the conversion is a two-degree polynomial function. The conversion from channel to energy is not necessary for the fitting procedure. The fitting routine is carried out on channels and at the end the fitted positions are converted for strain calculation. An asymmetric Pseudo-Voigt function is used for peak fitting. The background is estimated using a linear function. Other functions could be added in the future for both peak modelling and background estimation. One peak or multiple peaks can be fitted. The strains in the measurement direction are calculated using equation (4), followed by the calculation of the respective stress values.

While the technical setup at beamline ID15A allows for ADD measurements with a monochromatic beam, there is currently no dedicated software implementation at the beamline that would allow these measurements. Furthermore, to achieve depth resolution a conical or a spiral slit has to be used to define the gauge volume. The development is foreseen in the future. Generally, the workflow for strain/stress measurements with a 2D detector setup using monochromatic radiation include data integration and caking of the Debye-Scherrer rings, followed by fitting of the diffraction peaks. Strain and stress determination can be performed using the $\sin^2\psi$ [27] method or the fundamental method [28].

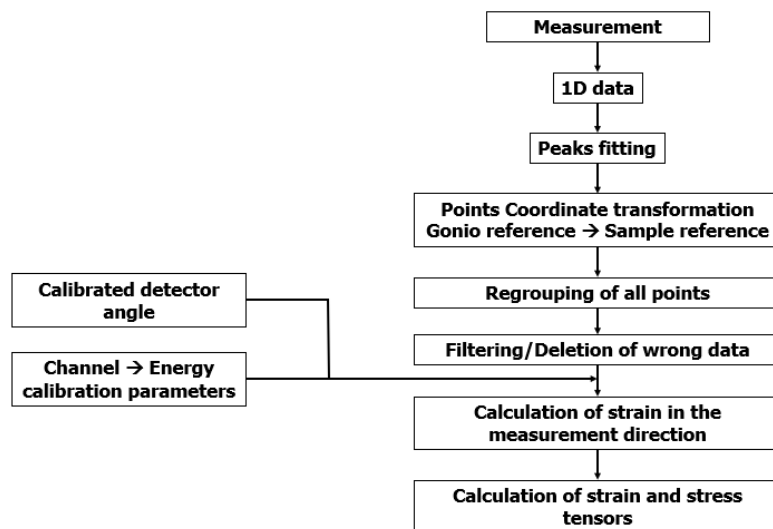


Figure 12. Data analysis workflow for residual stress determination using energy-dispersive synchrotron X-ray diffraction on ID15A with a 1D detector setup.

Currently, there is no automatic process in place that writes the processed data according to the NXstress format into a NeXus file. A first example for a data sets measured at beamline ID15A was converted via a python script specifically written by ESRF for this application.

3.3.2 P07 - High-Energy Materials Science Beamline (HEMS)

The High Energy Materials Science Beamline (HEMS) P07 at PETRA III is a monochromatic beamline for diffraction with high-energy photons. Measurements at P07 include both simple transmission geometry and depth-resolved residual stress analysis with conical slits. P07 comprises two experimental hutches EH1 and EH3. EH3 is the main experimental hutch and EH1 is a side station that serves for feasibility tests, detector testing, education of students, and in-house research. The

schematic of the main components of EH1 and EH3 is shown in Figure 13. For EH3, i.e. the main beam, the optics consist of two bent Si (111) Laue crystals (the first one water-cooled) on Rowland geometry (35.36° asymmetric cut, triangularly shaped with base 35 mm, length 89 mm and each 1.25 mm thick) in fixed exit (horizontal deviation 21 mm) keeping the beam at 1400 mm height above the floor. The energy is tuneable between $\sim 30\text{--}200$ keV with this double crystal monochromator (DCM) in horizontal scattering geometry. The maximum beam size is $1 \times 1 \text{ mm}^2$. The experimental hutche EH3 has a custom-built hexapod for heavy loads up to 1000 kg with positioning resolution of $\pm 1 \text{ }\mu\text{m}$ (travel ranges tens of cm, tilt angles up to 15°). This hexapod provides the spatial sample movements in x, y, and z directions and a separate table allows rotations of $\pm 180^\circ$. Conical slit cells (CSC) can be used for defining a gauge volume fixed in space. A small hexapod (identical to the EH1) allows the alignment of the CSC (fully orthogonal to the beam and with the beam passing through its centre). CSC can be used in both hutches, EH1 and EH3, requiring customized slit radii for their use with material exhibiting BCC, FCC, and HCP lattices. The focal distance, i.e. the distance between the conical slit and the centre of the gauge volume, is 100 mm.

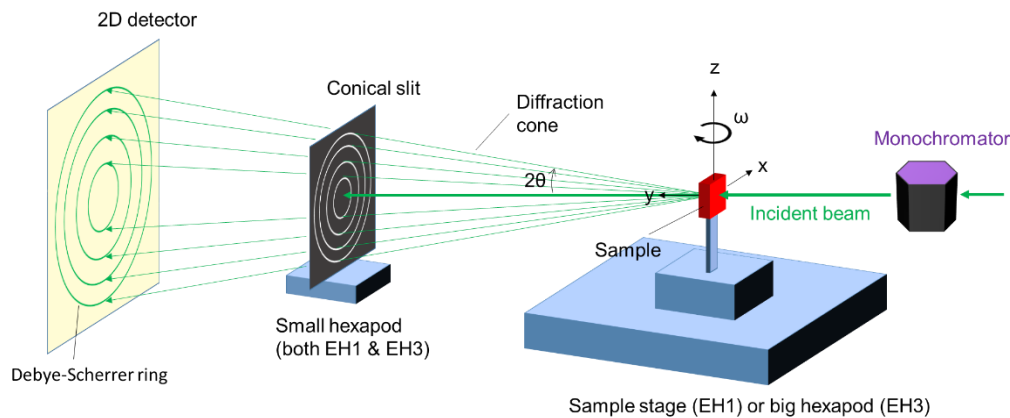


Figure 13. Schematic showing the components as well as the measurement and instrument axes of the ADD setup with a monochromatic beam at beamline P07 using a 2D detector setup. The setup is used in both hutches EH3 and EH1.

The optics for the side station (EH1) consist of two flat water-cooled Laue crystals Si (111) and Si (220) 15 mm (wide) \times 30 mm (high) \times 1.5 mm (thick) on a lateral slide, with an asymmetric angle 35.36° . The energy with this single bounce monochromator can thus be switched between 53.7 and 87.1 keV (scattering angle fixed to horizontally 4.25°). The maximum beam size is approximately $1 \times 1 \text{ mm}^2$. The instrumentation is composed of a mini-hexapod for the conical slit adjustment and a stage which permits a sample movement in the x and z directions. Additionally, two stages can be added for sample movement in y direction and sample rotation around the z axis which facilitates the sample alignment in the x-y plane, respectively.

For both hutches, EH1 and EH3, sample oscillation is also enabled in x or z directions to increase statistics during the measurements. In addition, an in-house built detector portal allows the use of various 2D-detectors (Varex XRD 4343, PerkinElmer XRD 1621, PILATUS3 X CdTe 2M, and mar345 image plate). Most commonly used are the PerkinElmer and Varex detectors with an array of 2048×2048 pixels and a pixel size of $200 \text{ }\mu\text{m}$ and an array of 2880×2880 pixels and a pixel size of $150 \text{ }\mu\text{m}$, respectively.

A flowchart describing the data analysis workflow of P07 is presented in Figure 14. The 2D images of the PE detector are recorded as “Tiff” files (dark images are subtracted) together with a metadata file that includes the exposure time, the number of exposures summed, the image number, and the time

at which it was saved. These images are subsequently integrated in different sectors aiming at calculating the strains at different ψ angles. Typically, sectors of 10° to 20° size at positions of 0° , 90° , 180° , 270° in ψ are evaluated (Figure 18 b). A commonly used software is Fit2D [29]. Sample positions (only in the scanned line or plane) are saved in a log file and they always refer to an absolute system defined before the experiment, i.e. the sample reference points (edges, centre of the sample...) have to be written manually and used as references in the data analysis.

Once the sectors are integrated, the Intensity vs 2θ diffractograms are obtained and the selected peak can be fitted using typical peak shape function such as Gaussian, Voigt, and Pseudo-Voigt. As the peak position is recorded in 2θ values, strains are calculated using equation (2), and stresses can be determined accordingly.

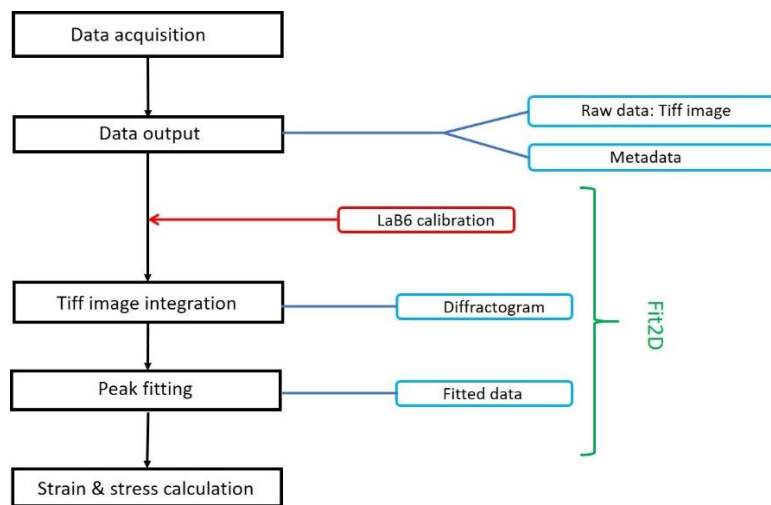


Figure 14. Data analysis workflow for residual stress determination using synchrotron X-ray diffraction on P07 beamline.

A NeXus file for the beamline P07 is currently under development. Metadata are not available as for beamline P61A. Nevertheless, since a data converter from beamline P61A is already available, the P07 data will be exported in a similar way.

3.3.3 P61A - White Beam Engineering Materials Science Beamline (WINE)

The beamline P61A is optimized for energy-dispersive residual stress analysis. The main components are similar to that of ID15A, and the schematic is illustrated in Figure 15. The incident synchrotron radiation results in a high intensity beam with energies ranging from 30 to 200 keV. Stress measurements on small samples are performed using the Eulerian cradle. A heavy-load diffractometer can be used for larger samples and sample environments. During a stress measurement, the energy dispersive detector positions define spatially the scattering vector directions, one for each detector. Two high purity Ge-detectors can be used simultaneously and independently positioned at any azimuth angle with a 2θ between 0° and 12° . Therefore, the instrument is able to measure strains in two linearly independent directions at the same time, reducing the number of acquisition points necessary for a stress scan. Both detectors are equipped with 0.5 m long double slit collimators. The sample is scanned regarding this vector and peak positions are collected for all energies at each point. These experiments can be performed in both transmission and reflection geometries. Stress measurements are typically done using the $\sin^2\psi$ method. A sketch of the Eulerian cradle nomenclature (Φ, χ, ω) together with the two-detector setup for a measurement is shown in the inset of Figure 15. The setup also allows for variation of angle of incidence (θ).

A flowchart describing the data analysis workflow of P61A is depicted in Figure 16. At beamline P61A, diffractograms are saved as “NeXus.nxs” files and metadata as FIO “fio” text files. All stages of the data analysis are handled using the in-house software P61A::Viewer [31]. The Viewer can perform three steps: (1) data corrections and conversion to energy scale; (2) displaying data in 2D or 3D plots; and (3) fitting selected peaks in a sequence of data.

Peaks can be automatically searched on multiple spectra or inserted manually in the subject project files. Every peak has a set of refineable parameters: centre, amplitude, sigma, etc., and a set of non-refineable parameters. The peak shape model function used is Pseudo-Voigt. The software can also be used to identify phase and hkl information for each peak. This information can be exported into the fit results file (“CSV” file format). The peak position information is saved as a function of energy, therefore strains are calculated using equation (4), and stress can be determined accordingly using the fundamental method. Alternatively, stresses can be determined using the $\sin^2\psi$ method which requires a conversion from energy to interplanar distance and a subsequent use of equation (2).

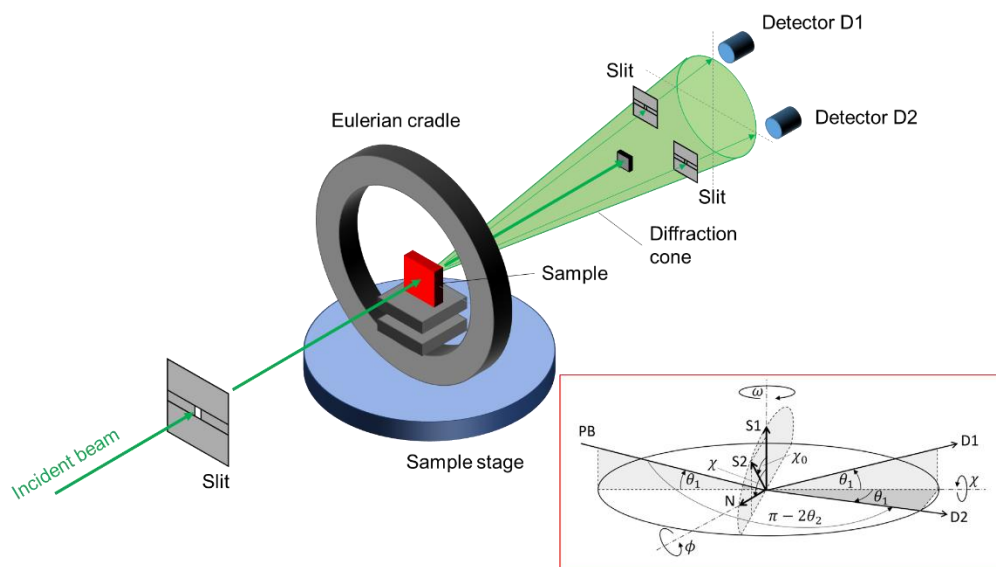


Figure 15. Illustration showing the setup of beamline P61A with the Eulerian cradle nomenclature in the insert (reproduced from [30]).

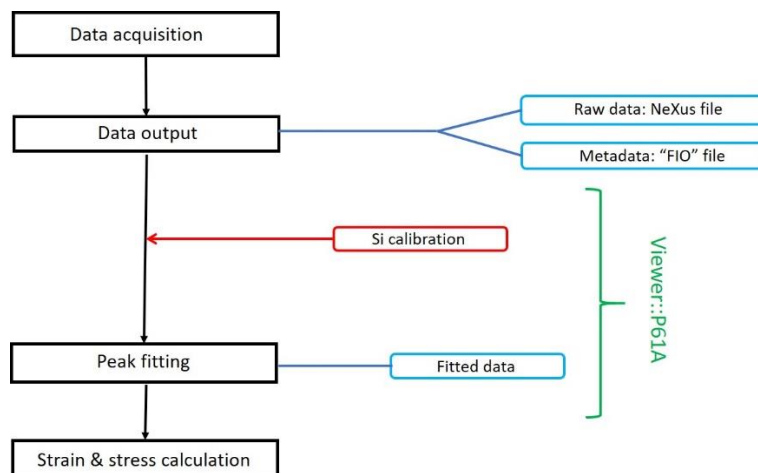


Figure 16. Data analysis workflow for residual stress determination using synchrotron X-ray diffraction on P61A.

A NeXus file following the NXstress format has already been created for the beamline P61A as a proof of concept that takes into account all particularities of this beamline.

4. Discussion

In the above sections, we have described the basic theory for RS analysis by neutron, synchrotron X-ray, and laboratory X-ray methods. In particular laboratory X-ray techniques use commercial equipment that is sold together with software packages that process the data more or less automatically from the measured raw data to the final stress values. This means that the integration of the (raw) data processing from laboratory X-ray instruments into the proposed NeXus-stress format as an input for the common software is too complex at the moment for the partner institutions (DTI, CETIM etc) and requires the direct engagement of the equipment and software developers. Eventually, an option would be to harmonize similar output files for RS values to compare this data to the common RS software in order to visualize results together with neutron and synchrotron ones. At the time of this deliverable both of these options seem to be feasible. With that said, we propose to compare the calculated stress values from laboratory X-ray measurement with synchrotron and neutron output in similar format (HDF5 or ASCII). Note that this will only include strain/stress values and xyz locations of the measurement. In order to interpret a sensible correlation, further information such as GV description and wavelength calibration will be requested from the laboratory X-ray operator/responsible before conclusions may be drawn. A similar case will be made for the comparison of the industrial FEM of RS addressed in WP5 (NEMAK, EDF, ArcelorMittal, etc).

Therefore, the subsequent focus of the data processing and harmonization lies on LRIs. Figure 17 summarizes and illustrates the data analysis workflow at all the above described LRI beamlines and instruments prior to the strain determination and stress calculation. It can be observed that all instruments have a similar data analysis workflow, i.e. raw data is reduced to obtain the diffractogram (which comprises Bragg peaks), the peaks are then fitted using an analytical model to obtain the accurate peak positions as input for strain and stress analysis including error calculations.

That said, each instrument saves the raw data and metadata, as well as the fitted peak results, in an individual way. It can also be observed that the data reduction, required to produce the diffractograms, is different for each instrument. The reason is that, despite the similarities of the method, hardware and measuring geometry are very instrument specific. In addition, while the participating instruments and beamlines have certain amount of freedom of how to process and save their data, at some facilities there are also in-house policies in place that dictate, for instance, the use of specific data reduction software (e.g. Mantid at ILL).

Therefore, the data reduction process from raw instrument data to diffraction peak analysis will remain the responsibility of the LRIs which also guarantees that any future instrumental updates are taken into account. However, the output data format, which is the input data format for our common software, shall be harmonized. Setting the specifications for this data format is the goal of Task 4.2.

Some examples shall illustrate this decision.

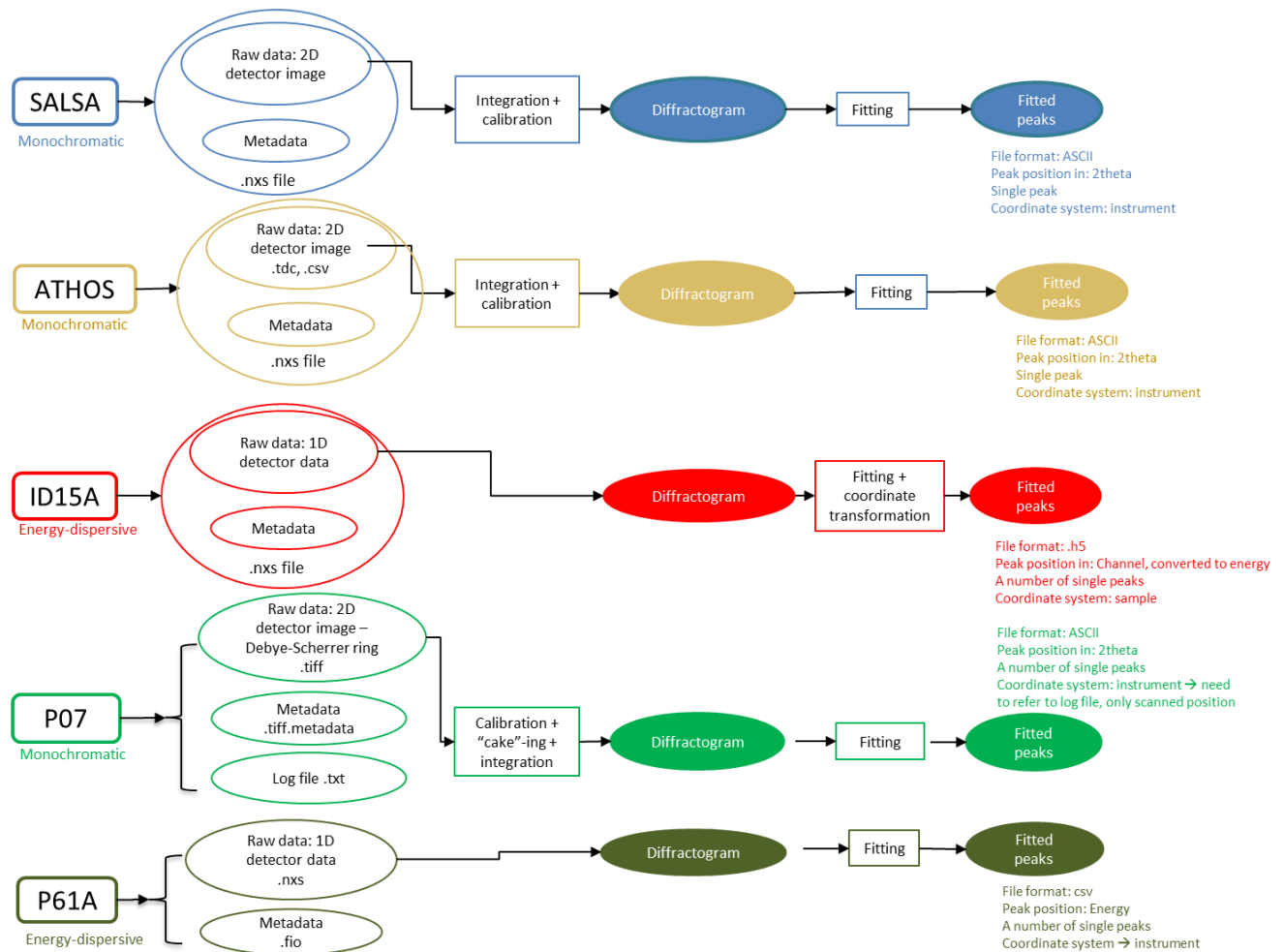


Figure 17. Summary of the data analysis workflow up to data reduction and data fitting at the participating beamlines.

The main difference between instruments is the detection system. For example, ATHOS and SALSA use a 2D PSD that covers a small range in 2θ . Therefore, the detector only captures a section of the Debye-Scherrer ring, requiring its data reduction a “straightening” of the curved ring-section followed by an integration across the detector height; see Figure 18(a). On the other hand, one setup at ID15A and at P07 uses 2D detectors positioned orthogonally to the beam which capture the whole Debye-Scherrer rings. Sectioning in different “cake-pieces” is required to select the azimuthal angle of the Debye-Scherrer ring to be integrated to get the diffractogram, Figure 18(b). Also, another setup at ID15A and at P61A uses 1D energy-dispersive detectors, i.e. the raw data is already a diffractogram, Figure 18(c). For this reason, each instrument has developed, or is currently developing, instrument-specific data reduction and peak fitting routines to optimize their data analysis workflow considering also the flexibility needed for continuous upgrades of the instrumentation, hardware, and software of these beamlines.

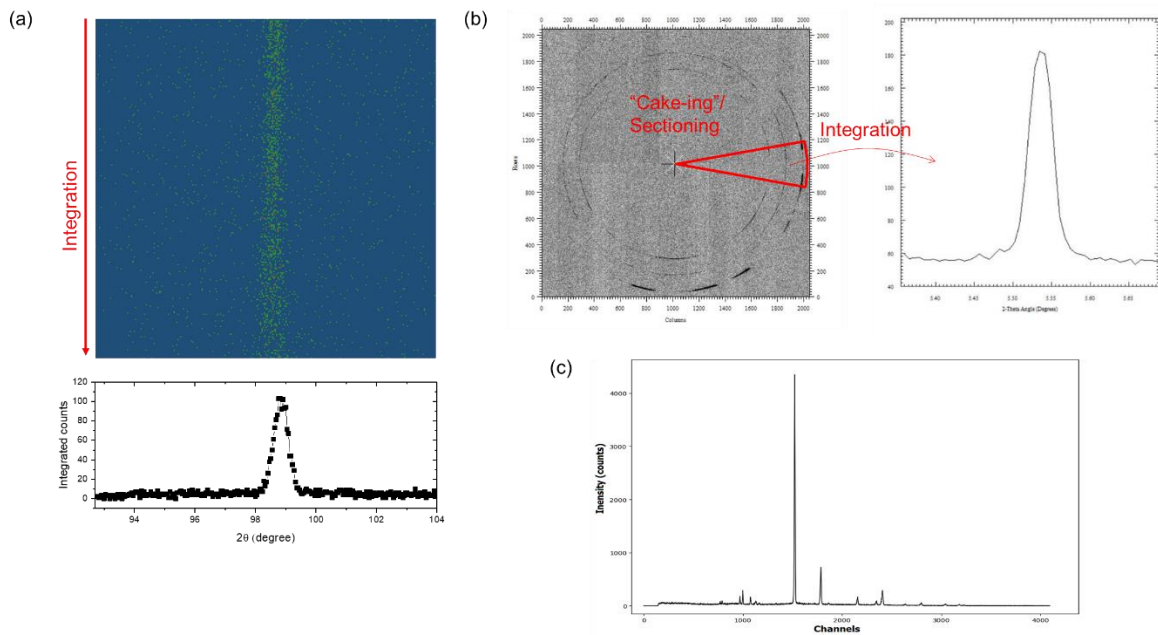


Figure 18. Illustration of data reduction processes to obtain a diffractogram for different types of detectors: (a) 2D PSD detector is integrated over the detector height; (b) Azimuthal angle sectioning followed by radial integration for 2D detector; (c) no integration required for 1D energy-dispersive detector.

5. Proposed harmonisation of analysis workflow and comparison with FE modelling

As mentioned in the introduction, the aim of WP4 and in particular of D4.2 is to establish standard workflows and algorithms for the data analysis of residual stress measurements performed at LRIs and compare them with laboratory X-ray measurements and FEM by providing a common RS software and a compatible data output format for the residual stress results. As described in the previous section, there are some stages in the data analysis workflow that are dependent on instrumentation and require a unique approach and tool for each instrument. It is therefore necessary to find a common point where the data analysis stage can be harmonised from which on a common software can be used. In this section, the proposed harmonisation and its justification is described. The common data format, the algorithm, and mathematical formulation behind the common software are also detailed. Note that the concept presented here is a working document and minor changes in the details of the data analysis workflow and its output are expected until the delivery of the software in March 2023 and at the end of the project in December 2023. Particularly a section of sustainability of this common software after EASISTRESS and transformation to the NXstress file format from other instruments outside the consortium are currently under discussion.

5.1 Proposed harmonization of data analysis

Figure 19 illustrates the generalized data analysis workflow of residual stress determination at the LRIs proposed in this work. Raw data and metadata format are produced according to the requirements and the setup of each instrument. Standard documents such as the ISO 21432:2019 and EN 15305:2009 provide recommendations on the parameters which are needed to be recorded in the raw data/metadata. Similar documents for synchrotron X-ray measurements are currently being developed by WP3 and WP6 of the EASI-STRESS project.

Data reduction and data fitting are to be handled by each instrument-specific data reduction software. By doing so, the development of this software can be independent, thus tailored to the requirements and demands of each instrument and setup. The data reduction and fitting process yield fitted data, typically a set of peak fitting parameters reporting peak position (in diffraction angle, neutron energy,

X-ray energy, or d-spacing), intensity, FWHM, among others. The fitted data output from different instruments share many common elements. Additionally, the data analysis algorithm required to bring the fitted data to strain and stress values are largely similar for all instruments. Therefore, metadata and fitted data are proposed to be harmonized as an input for the common software, i.e. the data file format and data structure will be standardized in the dedicated application NXstress [32]. The work of translating the instrument's fitted data output into the standardized format will use the resources of each facility; the present section serves as guidance and a responsible/contact will be nominated to support and validate this translation after the EASI-STRESS project. The standardized fitted data will become the input for the common software for residual stress determination developed within the EASI-STRESS project (denominated SOFT-EIS from now on as for SOFTWARE-Analyser for Industrial Stress). This common software will be responsible for calculating residual stress values and read and eventually display the metadata when requested for all instruments. Furthermore, its output will be aligned with industrial RS simulations in terms of content and formats.

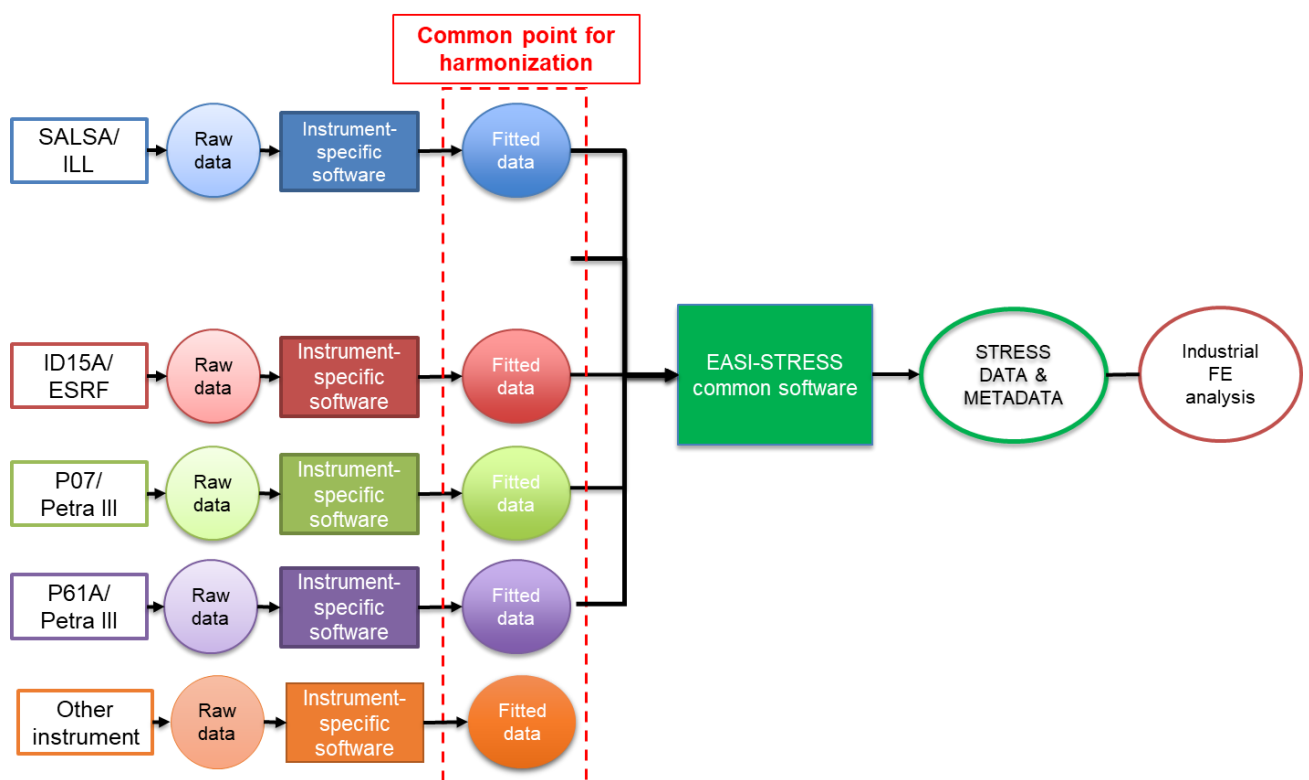


Figure 19. Diagram showing the common point for harmonisation of data analysis at different instruments proposed by the EASI-STRESS project.

5.2 Description of the harmonized fitted data input format

The proposed data output format from the instrument specific software is formulated with these considerations in mind:

- Data elements should comprise identifiers pointing to the experiment information. This will allow the data to be traced back to the original information from sample positioning, instrument setup, etc.
- Data elements should include information which captures the details of the data reduction and data fitting performed using the raw data. This will ensure the traceability of the data analysis workflow.
- Data structure should be arranged in such a way that it is easily readable by users and can be easily handled by the common software for further strain and stress determination.

- Data format should be easily amendable and expandable for future developments.

For these reasons, the hierarchical HDF5 file format was selected as the common data format. HDF5 is an open-source data format, and it uses a "file directory"-like structure which allows the organisation of data within the file in many different structured ways. Additionally, it supports heterogeneous and complex datasets to be stored, making it suitable for storing information ranging from simple comments as metadata to more complicated arrays which also include even pictures. A general, standardized HDF5 data format for the neutron, X-ray, and muon scientific communities (NeXus) already exists [19]. This is not specific for strain nor stress, but depending on the applications or measurement methods, different subclasses exist (e.g. small-angle scattering data, Electron backscatter diffraction (EBSD), and other diffraction patterns). During the EASI-STRESS project, a specific NeXus structure application definition for stress and strain analysis of crystalline material (NXstress) has been developed. A first version of its definitions is already publicly available [32]. Within the NXstress structure, certain entries have to be provided and are marked as "required". Lack of providing these entries will not allow the diffraction data to be treated in order to calculate strain and stress values. Additional entries in the NXstress format (marked either as "optional" or "recommended") are supplemental information that can be considered as meta data that allows to, for instance, trace the data processing procedures (by specifying e.g. paths or file names to calibration data), determine instrumental set-ups (by defining e.g. detectors), or specify additional information about the sample (by specifying e.g. the phase name or the space group). By choosing this generally used NeXus system, we guarantee sustainability of the format since there is an active international NeXus support group at multiple facilities that provides updates and upgrades on a regular basis. This ensures quick and easy adaptation upon, for example, instrument or method modifications, different RS software versions, etc.

To facilitate the description of the fitted data output format, a real measurement case is provided as an example. Figure 20 illustrates a measurement of the U-shaped sample at the SALSA instrument. Stresses in radial, tangential, and normal directions are to be characterized. The measurement points formed a line at the center of the bend, at the middle of the thickness of the sample. For each stress component, the measurement points were recorded in three separate raw data files, i.e. 046653-046655 for the radial component, 046695-046697 for the normal component, and 046720-046722 for the tangential component (Figure 20). These raw data files are then reduced and fitted using an instrument-specific data reduction software, in this case Mantid, to produce a fitted data file for each component, namely Fcompress_Line1_RADIAL, Fcompress_Line1_NORMAL, and Fcompress_Line1_TANGENTIAL, Figure 20.

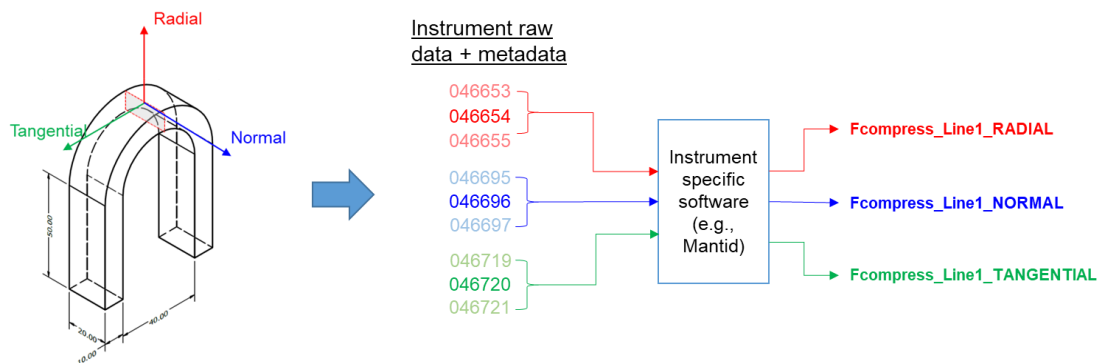


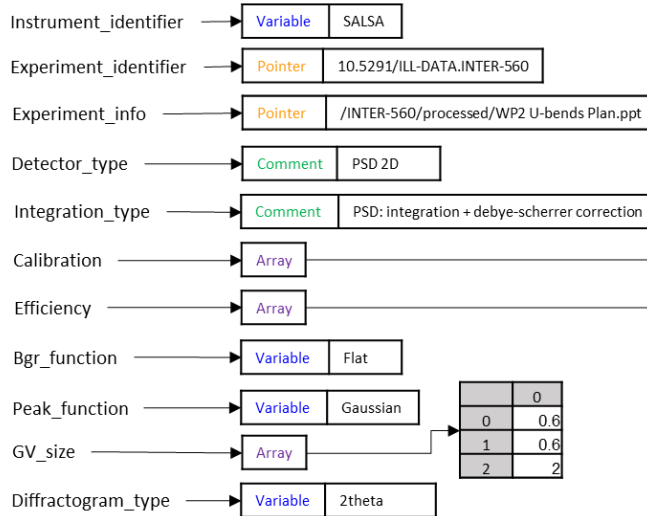
Figure 20. Illustration of the first stage of data analysis: raw data is reduced and fitted using instrument-specific data analysis software to produce standardised fitted data output.

The structure of each fitted data file is shown in Figure 21. Each file consists of a group termed “General_info”, and n-number of groups according to the number of measurement points included in the data file, termed “Point_0001”, “Point_0002”, ..., “Point_nnnn”. Each group consists of data elements, which are classified either as variable, pointer, comment, or array. Variables are strings which will trigger commands in the next stage of the data analysis (performed in the common software). Pointers are strings linked to folders or files in a separate directory. Comments are a simple descriptive text, while arrays are a matrix of values and variables.

Experimental and data analysis information relevant to all the measurement points are embedded in the “General_info”, Figure 21. “Instrument_identifier” is a variable related to the instrument being used, e.g., SALSA, ATHOS, ID15A, P07, or P61A. The group “Experiment_identifier” points to the digital object identifier (DOI) of the experiment. The group “Experiment_info” points to any file containing the details regarding the experimental design and setup (e.g. sample orientation, detailed information about the sample, etc.). While the group “Experiment_info” in the example illustrated in Figure 21 contains the link to a .ppt file, it could also be a .txt file or any other file format. The group “Detector_type” refers to the type of detector used in the instrument, e.g. PSD 1D, PSD 2D, image plate, single detector, TOF, energy-dispersive, etc. The group “Integration_type” is the raw data integration used in the data reduction process, e.g. Debye-Scherrer correction and integration for PSD, umbrella correction for single detector, segmentation positon for 2D plate detector, etc. “Calibration” is an array consisting of a lookup table that converts each detector channel into 2θ -angle, neutron energy, X-ray energy, or time-of-flight. “Efficiency” is a lookup table consisting of an efficiency factor for each detector channel. “Bgr_function” is a variable referring to the background function used for the peak fitting, and it can be a Flat, Linear, Quadratic, or Shape function. “Peak_function” is a variable describing the function used for the peak fitting, and it can be a Gaussian, Lorentzian, Pseudo-Voigt, etc. “GV_size” is an array containing the information regarding the dimension of the gauge volume (width, length, height). “Diffractogram_type” is a variable describing the type of spectrum used by the diffractogram, and it can be 2θ , energy, or d-spacing.

Fcompress_Line1_RADIAL

General_info



	0		0
0		0	
1		0	
2		0	
3		0	
4		0	
5		0	
6	1.187576		
7	1.148303		
8	1.136523		
9	1.132649		
...	...		

	0		0
0		-5.53802	
1		-5.4962	
2		-5.45426	
3		-5.4122	
4		-5.37002	
5		-5.32772	
6		-5.28531	
7		-5.2428	
8		-5.20017	
9		-5.15745	
...			

Point_0001

Point_0002

Point_0003

Point_0004

....

Point_nnnn

Fcompress_Line1_NORMAL

Fcompress_Line1_TANGENTIAL

Figure 21. Proposed data structure of the standardised fitted data output describing the “General_info” group.

Figure 22 illustrates the data elements contained in the Point_0001 group. These data elements are identical for all the “Point_nnnn” groups. “Raw_data_info” is a pointer linked to the original raw data files from which the corresponding measurement points are saved. The diffractogram measured at the corresponding point and the analytical fitting model are provided in “Diffractogram” and “Fitted_spectrum”, respectively. This information provides traceability of the data analysis and allows a visual inspection of the quality of the fit. The fitting parameter information is then provided in three groups: “Fit_parameter_name”, “Fit_parameter”, and “Fit_parameter_uncertainty”. The listed parameters will depend on the background and fitting function used in the analysis. Finally, the instrument and experiment variables that are recorded during the data acquisition of the corresponding measurement point are listed under “Variables”, “Variable_name”, and “Variable_unit”. As a minimum, it must include the position of the measurement point in the sample coordinate system (X, Y, Z), the instrument angles (e.g., 2θ , ω , ϕ , χ), the number of counts, and the counting time. Additional variables that are recorded during the measurement can be added, e.g. sample temperature or applied force, if applicable.

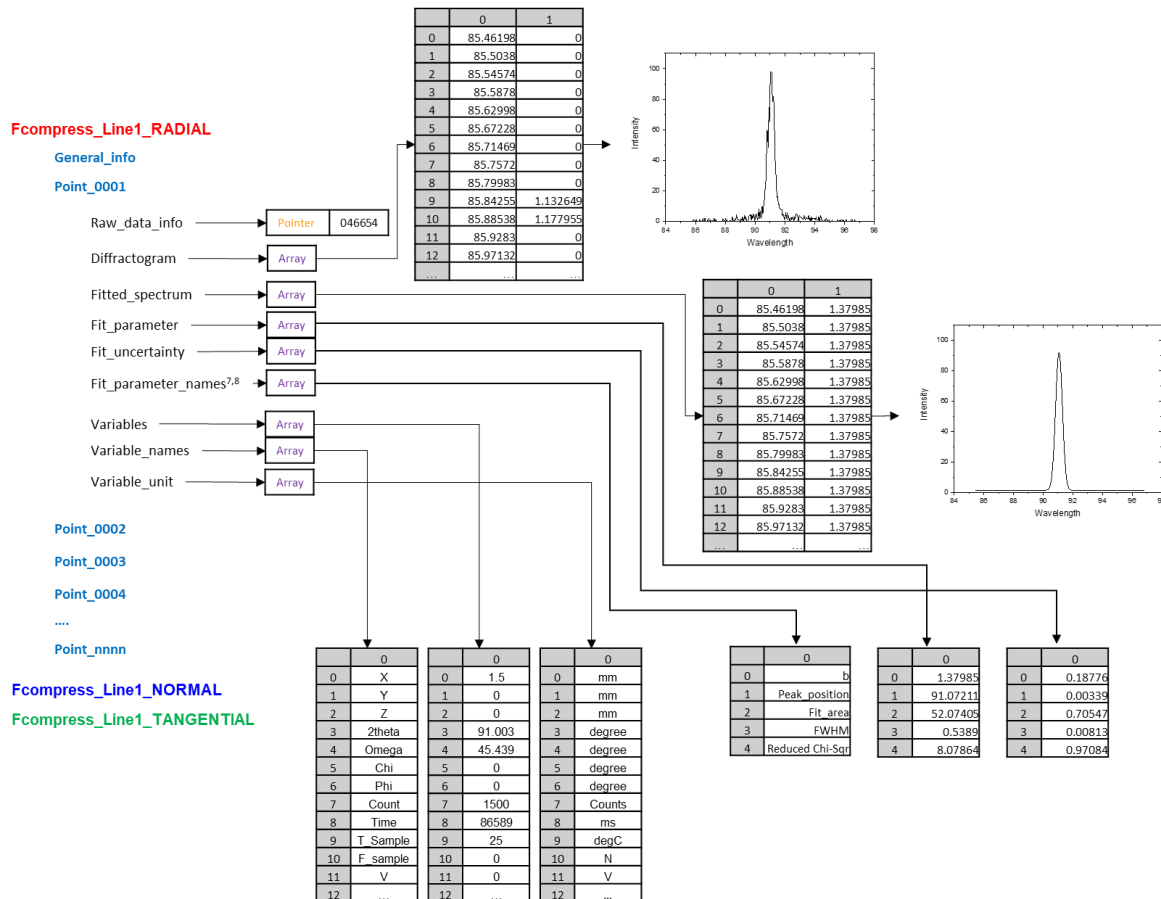


Figure 22. Proposed data structure of the standardised fitted data output describing the “Point_nnnn” group.

5.3 Algorithm and mathematical formulation of the common software for residual stress determination

This section describes the algorithm and the mathematical formalism that will be incorporated into the common software for the residual stress measurement developed in the framework of the EASI-STRESS project. The software will take the fitted data format described in the previous section as the input, and will produce a standardized residual stress data output which will be described in the next section. The first development of this software will focus on tri-axial stress measurement cases, and other extended cases (e.g. more than 6 strain components measured for the full stress tensor determination, *in-situ* characterization, etc.) will be developed in the future. The diagram describing the algorithm of the common software is presented in Figure 23, while each step of the data analysis including the mathematical formalism is illustrated in Table 3.

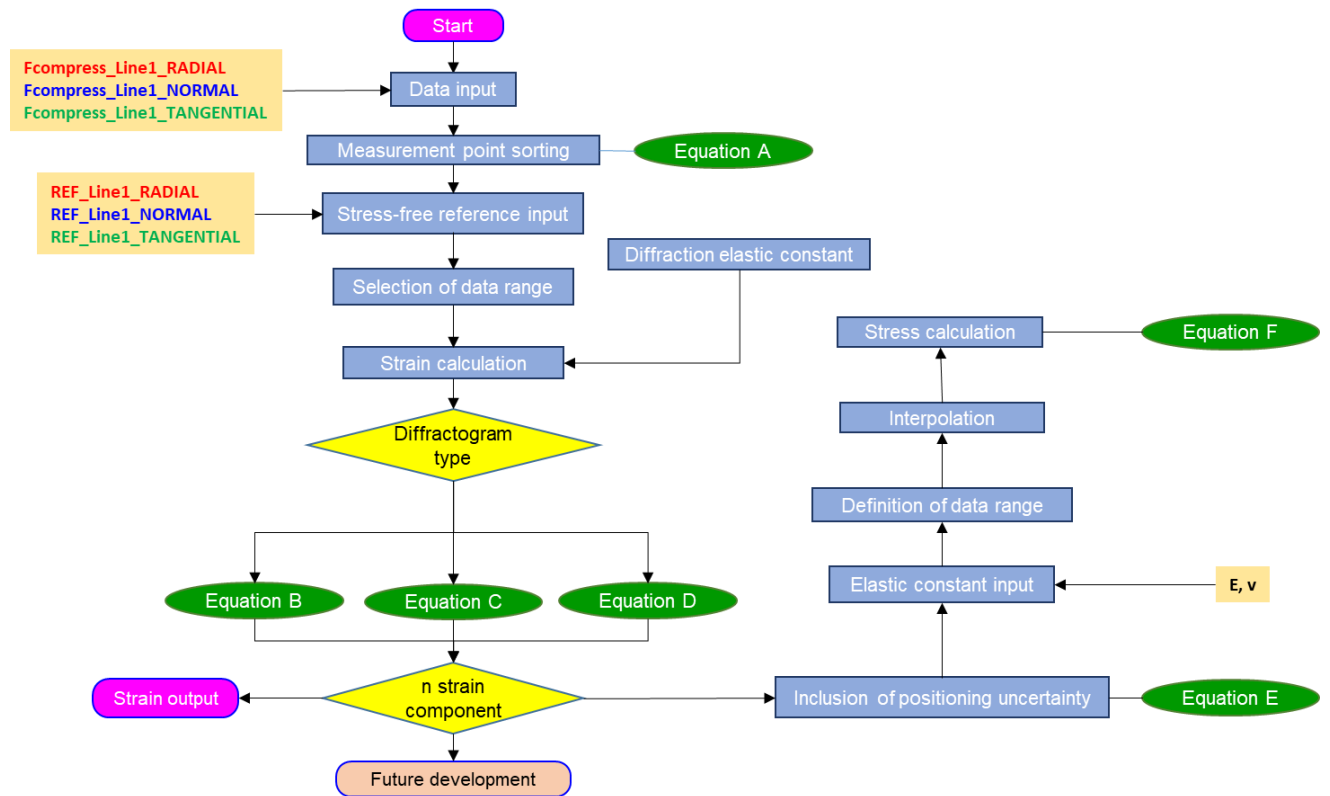
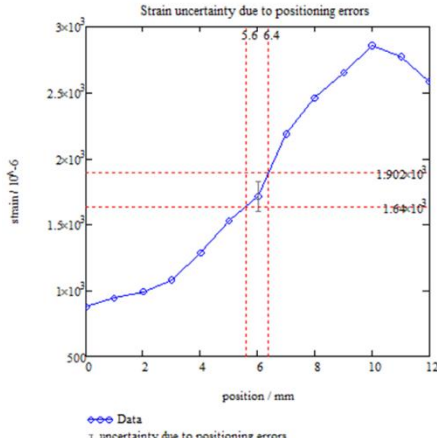
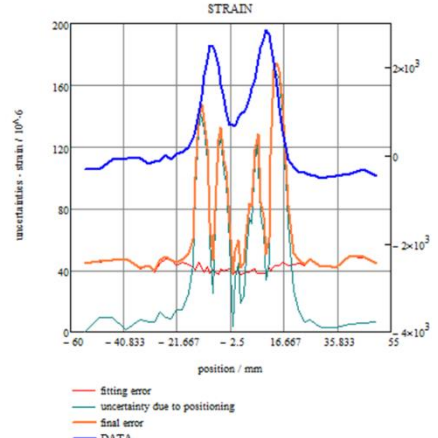


Figure 23. Diagrams of the data analysis workflow/algorithm for the common software for residual stress determination.

Table 3. Mathematical formulation of the common software.

Data analysis steps	Description and mathematical formalism
Data input	In the first step, the user is requested to input the measurement data, which are the fitted data of different components. Variables from each measurement point are read in, including sample coordinates X, Y, Z, diffraction angle 2θ , peak width, and peak amplitude with their corresponding uncertainties.
Measurement point sorting	Coordinates of measurement points should be already in the sample coordinate system. If it is still in the instrument coordinates, it needs to be converted by rotating the sample in the opposite way as during the experiment. Centre of rotation: C, coordinate (x,y,z). Translation to the centre: $\begin{pmatrix} X_i \\ Y_i \\ Z_i \end{pmatrix} \leftarrow \begin{pmatrix} x_i \\ y_i \\ z_i \end{pmatrix} - \begin{pmatrix} C_x \\ C_y \\ C_z \end{pmatrix} \quad (A1)$ During the experiment the sample had been rotated by α, β, γ Now rotate the coordinates backwards by $-\gamma, -\beta, -\alpha$: $\begin{pmatrix} X_i \\ Y_i \\ Z_i \end{pmatrix} = \begin{pmatrix} \cos(\gamma) & \sin(\gamma) & 0 \\ -\sin(\gamma) & \cos(\gamma) & 0 \\ 0 & 0 & 1 \end{pmatrix} \cdot \begin{pmatrix} \cos(\beta) & 0 & -\sin(\beta) \\ 0 & 1 & 0 \\ \sin(\beta) & 0 & \cos(\beta) \end{pmatrix} \cdot \begin{pmatrix} 1 & 0 & 0 \\ 0 & \cos(\alpha) & \sin(\alpha) \\ 0 & -\sin(\alpha) & \cos(\alpha) \end{pmatrix} \cdot \begin{pmatrix} x_i \\ y_i \\ z_i \end{pmatrix} \quad (A2)$

Stress-free reference input (d_0)	<p>The user is requested to input the stress-free reference data.</p> <p>The stress-free reference data can be in the form of:</p> <ul style="list-style-type: none"> i) one single value (i.e. powder sample or average of all/some orientations) ii) one single value for each orientation iii) a scan or gradient in 1D, 2D, or 3D in the case of compositional or microstructural gradients. Here, some level of interpolation of the measured d_0 location versus the scanned one in the sample may be considered. iv) a value dependent on time and/or external conditions such as temperature during in-situ studies
Selection of data range	Select data-range for further analysis. (One might want to exclude regions or measurement points)
Strain calculation	<p>The software reads the variable "Diffractionogram_type" from the fitted data file. Depending on the "Diffractionogram_type", the strain is calculated using the equations below. Subscript 0 refers to the stress-free reference. While not explicitly shown with an index, all the measurement components are directional, for example for tri-axial stress determination: xx,yy,zz.</p> <p>If Diffraction_type = 2theta</p> $\varepsilon = \frac{\sin \theta_0}{\sin \theta} - 1 \quad (B1)$ $\Delta \varepsilon = \sqrt{\left(\frac{-\cos(\theta) \sin \theta_0}{\sin(\theta)^2}\right)^2 \cdot \Delta \theta^2 + \left(\frac{\cos(\theta_0)}{\sin \theta}\right)^2 \cdot \Delta \theta_0^2} \quad (B2)$ <p>If Diffraction_type = Energy</p> $\varepsilon = \frac{E_0}{E} - 1 \quad (C1)$ $\Delta \varepsilon = \sqrt{\frac{1}{E} \Delta E_0^2 + \frac{E_0^2}{E^4} \Delta E^2} \quad (C2)$ <p>If Diffraction_type = d_spacing</p> $\varepsilon = \frac{d}{d_0} - 1 \quad (D1)$ $\Delta \varepsilon = \sqrt{\frac{1}{d_0^2} \Delta d^2 + \frac{d^2}{d_0^4} \Delta d^2} \quad (D2)$ <p>The number of independent strain directions to be measured depends on the assumptions on the stress field. For bi-axial (or plane) stress states, two components are sufficient since normal stress is zero. For tri-axial stress states three perpendicular directions need to be measured (most common application). For full strain / stress tensor determination requires at least six linearly independent components.</p>
Inclusion of positioning uncertainty	<p>For the stress calculation, in addition to uncertainties from the peak fitting, positioning uncertainties should be included. The importance of positioning uncertainties in the residual stress determination using neutron diffraction (also relevant for other diffraction techniques) was described in previous works [33,34]. This can be done as follows:</p>

	<p>Take the m-number of strain values in a region around the measuring point of width $2 \Delta x$, the positioning uncertainty, and calculate their standard deviation. (Values at the border of this range are interpolated).</p> $\text{StdDev} = \sqrt{\frac{\sum x^2}{m} - \left(\frac{\sum x}{m}\right)^2} \quad (\text{E})$ <p>Add the obtained standard deviation to the uncertainty value from the peak fitting:</p> $\Delta \varepsilon_x = \sqrt{(\Delta \varepsilon_x)^2 + \text{StdDev}(\Delta x_x, \varepsilon_x)^2}$ $\Delta \varepsilon_y = \sqrt{(\Delta \varepsilon_y)^2 + \text{StdDev}(\Delta y_x, \varepsilon_y)^2} \quad (\text{E})$ $\Delta \varepsilon_z = \sqrt{(\Delta \varepsilon_z)^2 + \text{StdDev}(\Delta z_x, \varepsilon_z)^2}$ <p>The graph in Figure 24 shows the influence of the positioning error on the final error estimation. In orange: the measured strain profile. In red: the uncertainty from peak fitting. It remains in a range between 40 μe and 50 μe. In green: the calculated standard deviation assuming positioning errors of 0.2 mm. Around relatively constant strain values the effect of positioning uncertainties is very small. But in the strain gradient interval the error can become significant. As a result, the combined error (blue line) is even twice as large as the fitting error in this example.</p> <p>ATTENTION: This calculation is only relevant for the estimation of stress uncertainties! The strain values have no positioning error.</p> <div style="display: flex; justify-content: space-around;">   </div> <p><i>Figure 24. Influence of the positioning error on the final error estimation.</i></p>
Elastic constant input	User input of the elastic constants $E_{x,y,z}$ and $\nu_{x,y,z}$ for each hkl and strain direction.
Definition of data range	Due to experimental constraints or restrictions, data points for different strain orientations do not always lie on the same coordinate. Therefore, some outermost points need to be excluded for stress calculation, others need to be interpolated. (See box below)
Interpolation	Take all locations of all data points for all orientations by linearly interpolating the values for the subsequent stress calculation. Measurement points in the different orientations are not necessarily all at the same location (different step size,

excluding outliers, no data obtained in some regions, entry scan and re-calculation of positions...). An example for a measurement of three strain components at different measurement points (within the same line) is shown below.

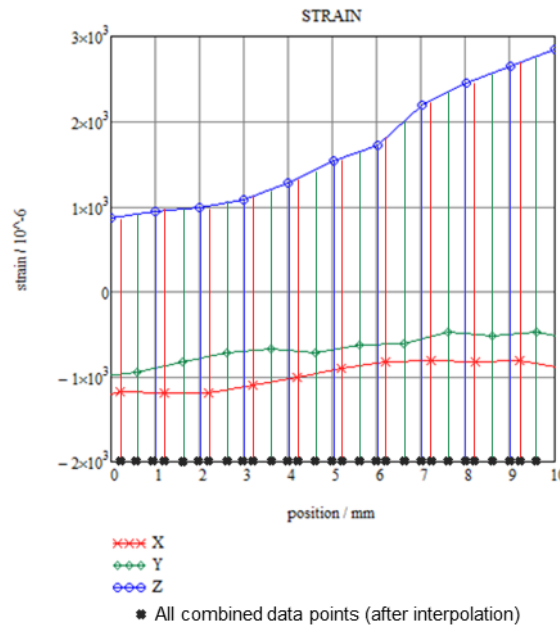


Figure 25. Illustration of the strain values at different measurement points.

In this example, including 10 measurement points in each x,y, and z orientation, 30 stress values will be calculated: at each single point of a strain measurement, the strain measurements of the other components will be linearly interpolated for the stress calculation.

Stress calculation

In the final stage, stresses are calculated. For tri-axial stress determination the following equation (F) are used.

Using the substitution factor S:

$$\begin{aligned} S_x &= \frac{E_x \cdot v_x}{(1 + v_x) \cdot (1 - 2v_x)} \\ S_y &= \frac{E_y \cdot v_y}{(1 + v_y) \cdot (1 - 2v_y)} \\ S_z &= \frac{E_z \cdot v_z}{(1 + v_z) \cdot (1 - 2v_z)} \end{aligned} \quad (F1)$$

Stresses are then calculated using the equation below (taking the combined strain uncertainties that include positioning uncertainties).

$$\begin{aligned} \sigma_x &= \frac{E_x}{1 + v_x} \cdot \varepsilon_x + S_x \varepsilon_x + S_y \varepsilon_y + S_z \varepsilon_z \\ \sigma_y &= \frac{E_y}{1 + v_y} \cdot \varepsilon_y + S_y \varepsilon_y + S_x \varepsilon_x + S_z \varepsilon_z \\ \sigma_z &= \frac{E_z}{1 + v_z} \cdot \varepsilon_z + S_z \varepsilon_z + S_x \varepsilon_x + S_y \varepsilon_y \end{aligned} \quad (F2)$$

For now, we implement and discuss only the specific case currently being used at participating LRI facilities without taking into account

uncertainties in elastic constants. In the case that measurements of all different components were independent, the Gaussian formalism for error propagation is used to calculate uncertainties in stress:

$$\Delta\sigma_x = \sqrt{\left[\frac{1 - \nu_x}{(1 + \nu_x) \cdot (1 - 2\nu_x)} \cdot E_x \cdot \Delta\varepsilon_x \right]^2 + (S_y \cdot \Delta\varepsilon_y)^2 + (S_z \cdot \Delta\varepsilon_z)^2}$$

$$\Delta\sigma_y = \sqrt{\left[\frac{1 - \nu_y}{(1 + \nu_y) \cdot (1 - 2\nu_y)} \cdot E_y \cdot \Delta\varepsilon_y \right]^2 + (S_x \cdot \Delta\varepsilon_x)^2 + (S_z \cdot \Delta\varepsilon_z)^2}$$

$$\Delta\sigma_z = \sqrt{\left[\frac{1 - \nu_z}{(1 + \nu_z) \cdot (1 - 2\nu_z)} \cdot E_z \cdot \Delta\varepsilon_z \right]^2 + (S_x \cdot \Delta\varepsilon_x)^2 + (S_y \cdot \Delta\varepsilon_y)^2}$$

In case there is a correlation between strain values, as this is true when the same reference value is used, the covariance between values has to be taken into account. From the extended Gaussian error propagation, we obtain:

$$\Delta\sigma_x = \left| \left(\frac{E_x}{(1 + \nu_x)} + S_x \right) \Delta\varepsilon_x + S_y \cdot \Delta\varepsilon_y + S_z \cdot \Delta\varepsilon_z \right|$$

$$\Delta\sigma_y = \left| \left(\frac{E_y}{(1 + \nu_y)} + S_y \right) \Delta\varepsilon_y + S_x \cdot \Delta\varepsilon_x + S_z \cdot \Delta\varepsilon_z \right|$$

$$\Delta\sigma_z = \left| \left(\frac{E_z}{(1 + \nu_z)} + S_z \right) \Delta\varepsilon_z + S_y \cdot \Delta\varepsilon_y + S_x \cdot \Delta\varepsilon_x \right|$$

A bi-axial stress state, stresses can only be calculated by assuming that the missing component has minimum strain values (plane strain) or has values similar to the other component. The condition of plane-stress is generally assumed for thin plates or surface layers. The stress distribution is then defined by the principal stresses σ_{11} and σ_{22} in the plane of the surface, which also means that there does not exist a stress perpendicular to the free surface. Therefore, the normal stress component σ_{33} as well as the shear stresses $\sigma_{13} = \sigma_{31}$ and $\sigma_{23} = \sigma_{32}$ facing out of the plane of the sample are equal to zero. However, there exists a corresponding strain component perpendicular to the surface, ε_{33} , which results from the Poisson's ratio contractions caused by two principal stresses. **Otherwise, strain data can be produced as output.** If 6 components or more are measured, the full strain and stress tensors can be determined. This will be implemented in the future development of the software.

The equivalent Von Mises stress can be calculated as follows:

$$\sigma_{vm} = \frac{1}{\sqrt{2}} \sqrt{(\sigma_x - \sigma_y)^2 + (\sigma_y - \sigma_z)^2 + (\sigma_z - \sigma_x)^2 + 6(\tau_{xy}^2 + \tau_{yz}^2 + \tau_{zx}^2)}$$

There, shear stresses can be calculated as a function of the normal stresses using the lame constants:

$$\mu = \frac{E}{2(1 + \nu)}$$

$\tau_{xy} = 2\mu\epsilon_{xy}$ $\tau_{yz} = 2\mu\epsilon_{yz}$ $\tau_{xz} = 2\mu\epsilon_{xz}$ <p>However, for the general case where strain scanning shear stresses are usually omitted assuming only principal strain/stress directions in x,y,z coordinate system the Von Mises calculation is:</p> $\sigma_{vm} = \sqrt{\frac{1}{2} \cdot [(\sigma_x - \sigma_y)^2 + (\sigma_y - \sigma_z)^2 + (\sigma_z - \sigma_x)^2]} \quad (F3)$ <p>Uncertainties in the Von Mises stress are obtained from the following calculation:</p> $\Delta\sigma_{vm} = \sqrt{\frac{(2 \cdot \sigma_x - \sigma_y - \sigma_z)^2 \cdot (\Delta\sigma_x)^2 + (2 \cdot \sigma_y - \sigma_x - \sigma_z)^2 \cdot (\Delta\sigma_y)^2 + (2 \cdot \sigma_z - \sigma_x - \sigma_y)^2 \cdot (\Delta\sigma_z)^2}{2 \cdot [(\sigma_x - \sigma_y)^2 + (\sigma_x - \sigma_z)^2 + (\sigma_y - \sigma_z)^2]}}$
--

5.4 Description of the final residual stress data output format

As a result of the data analysis workflow, the residual stress data output can be produced. The main focuses for the definition of residual stress data output are: i) traceability of the experiment and data analysis, and ii) suitability of the data for input in industrial finite element analysis. As mentioned in the text above, traceability has been integrated into the development and harmonisation of the data analysis workflow by including important information and parameters relating to the experimental and data analysis details. On the other hand, a required data structure suitable for FE analysis activities has been defined in EASI-STRESS work package 5 (WP5). This definition is taken into account in this work.

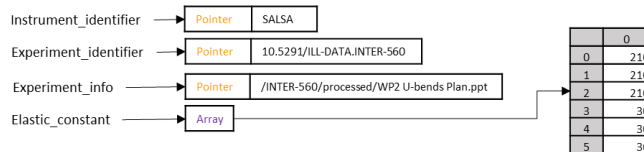
Figure 26 shows the overall structure of the residual stress data output proposed in this work. For the same reasons as used for the fitted data output format, the hierarchical file format HDF5 was suggested as the output data format. However, a large part of the user community, whether academic or industrial, lack capabilities to process files in this data format. Therefore, another output file format will be simple ASCII files. The residual stress data output in the HDF5 comprises three groups, namely "General_info", "Stress_output", and "Strain_output". Similar to the fitted data input file, the "General_info" group of the residual stress data output includes pointers to the instrument used for the experiment, to the experiment, and to the file containing the experimental details, respectively termed "Instrument_identifier", "Experiment_identifier", and "Experiment_info". In the same group, an array, called "Elastic_constant", includes the elastic constant values (Young's modulus and Poisson's ratio) for each strain component.

The "Stress_output" group contains the main information about the residual stress measurement data in "Variable", "Variable_uncertainty", "Variable_name", and "Variable_unit". The variables included in the residual stress output data are measurement point number, measurement point coordinates (in the sample coordinate system), stress values in the different components, the precise dimensions of the gauge volume and its orientation with respect to the sample, and corresponding uncertainties. According to the work of EASI-STRESS WP5, the inclusion of these variables ensures the compatibility of the residual stress calculation output from the LRIs as input for industrial FE modelling activities and comparison of results.

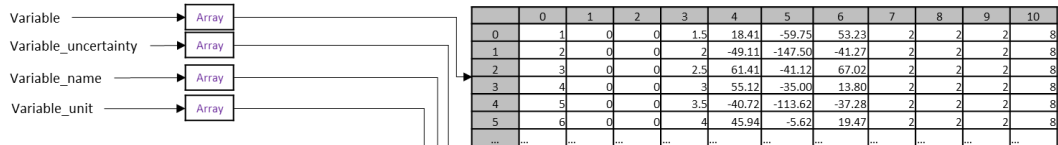
The final group is labelled “Strain_output”, which contains n -number of subgroups according to the number of measured strain components for the stress determination ($n = 3$ for tri-axial stress determination). Each subgroup contains a pointer to the fitted data file, labelled “Data_file”. The pointer “Reference_file” refers to a separately fitted data file in case a stress-free reference trend was used to calculate the strains (“None” if the reference is a single value). Meanwhile, the variable “Reference_value” refers to a value that is used as the stress-free reference (“None” if the reference is a trend, Figure 26). The main strain information is stored in “Strain_variable” and “Strain_variable_name”. They contain the coordinates of measurement points (in the sample coordinate system), the strain values, and the strain uncertainties.

Stress_output_FCompress

General_info

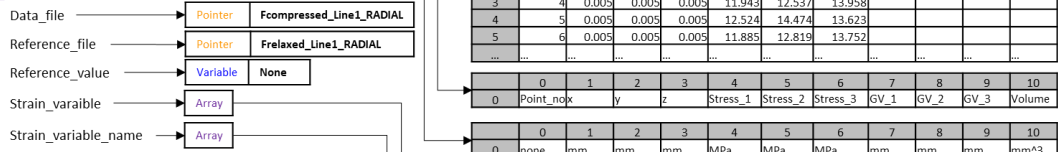


Stress_output



Strain_output

Strain_01



Strain_02

Strain_03

	0	1	2	3	4
0	0	0	1.5	96.998	34.003
1	0	0	2	35.817	29.238
2	0	0	2.5	255.437	35.803
3	0	0	3	292.785	34.176
4	0	0	3.5	21.679	35.608
5	0	0	4	198.961	33.863

	0	1	2	3	4
0	X	Y	Z	Strain	Strain error

Figure 26. Output format of the calculated stress values in the HDF5 file.

6. Summary and Outlook

In this document we have described the mathematical formalism for calculating strain and stress based on data collected at participating LRIs. The currently available neutron instruments and synchrotron beamlines within the EASI-STRESS project, including their measurement workflow and data processing procedures, have been described. For the harmonization of the data produced at LRIs, which will be the input for the common software, the NeXus file format was chosen and a new application (NXstress) specifically for strain and stress was developed and outlined. We have further described the minimum set of equations that will be used in the common software for strain and stress calculations as well as the first working mechanism and structure of the software. The next steps will be to describe in more depth the special measurement cases and compile equations and workflows that should be included in the common software. We have also drafted the structure of the output files from the common software specifically for the HDF5 format. Since this is not the preferred format

by the user community yet, we are also working on the implementation of a structure of ASCII output files based on the information from the deliverable D5.1.

7. References

- [1] A.J. Allen, M.T. Hutchings, C.G. Windsor & C. Andreani (1985) Neutron diffraction methods for the study of residual stress fields, *Advances in Physics*, 34:4, 445-473, DOI: 10.1080/00018738500101791
- [2] G.A. Webster, A.N. Ezeilo (1997) Neutron scattering in engineering applications, *Phys. B Condens. Matter* 949–955. DOI: 10.1016/S0921-4526(96)01221-5.
- [3] VAMAS report by G.A. Webster (2000) Neutron Diffraction Measurements of Residual Stress in a Shrink- fit Ring and Plug. ISSN 1016-2186
- [4] R.S. Ramadhan, S. Cabeza, T. Pirling, S. Kabra, M. Hofmann, J. Rebelo Kornmeier, A.M. Venter, D. Marais. (2021) Quantitative analysis and benchmarking of positional accuracies of neutron strain scanners. *Nuclear Instruments and Methods in Physics Research Section A: Accelerators, Spectrometers, Detectors and Associated Equipment.*, Volume 999, 165230, ISSN 0168-9002, DOI: 10.1016/j.nima.2021.165230.
- [5] Reimers, W., Broda, M., Brusch, G. et al. Evaluation of Residual Stresses in the Bulk of Materials by High Energy Synchrotron Diffraction. *Journal of Nondestructive Evaluation* 17, 129–140 (1998). <https://doi.org/10.1023/A:1022607030355>
- [6] NPL-National Physical Laboratory (2005). Measurement Good Practice Guide No. 52: Determination of Residual Stresses by X-ray Diffraction – Issue 2. M.E. Fitzpatrick, A.T. Fry, P. Holdway, F.A. Kandil, J. Shackleton and L. Suominen. ISSN 1744-3911.
- [7] ISO 21432:2019 Non-destructive testing — Standard test method for determining residual stresses by neutron diffraction
- [8] International Atomic Energy Agency — IAEA. Development and Applications of Residual Stress Measurements Using Neutron Beams, Technical Reports Series No. 477, IAEA, Vienna (2014)
- [9] Neutron Quality Label: trademark number #018531682 – by the European Union Intellectual Property Office (EUIPO). The Neutron Quality Label mark is filed in the category of Education and Entertainment Services, Computer & Software Services & Scientific Services and is property of Institut Max von Laue - Paul Langevin.
- [10] EN 15305:2009 Test Method for Residual Stress analysis by X-ray Diffraction
- [11] Epp, J. 4 - X-ray diffraction (XRD) techniques for materials characterization. In *Materials Characterization Using Nondestructive Evaluation (NDE) Methods*, Hübschen, G., Altpeter, I., Tschuncky, R., Herrmann, H.-G. Eds.; Woodhead Publishing, 2016; pp 81-124.
- [12] Lorentzen, T.; Christoffersen, J. Limitations on the strain tensor determination by neutron diffraction using a position-sensitive detector. *NDT International* **1990**, 23 (2), 107-109.
- [13] Tanaka, K. The $\cos\alpha$ method for X-ray residual stress measurement using two-dimensional detector. *Mechanical Engineering Reviews* **2019**, 6 (1), 18-00378-00318-00378.
- [14] Pham, T.-Q.-S.; Geandier, G.; Ratel-Ramond, N.; Mareau, C.; Malard, B. X-Light: an open-source software written in Python to determine the residual stress by X-ray diffraction. *J Appl Crystallogr* 2021, 54 (4)

- [15] Ferrari, M.; Lutterotti, L. Method for the simultaneous determination of anisotropic residual stresses and texture by x-ray diffraction. *J Appl Phys* **1994**, 76 (11), 7246-7255.
- [16] Lutterotti, L.; Matthies, S.; Wenk, H.-R. MAUD (material analysis using diffraction): a user friendly Java program for Rietveld texture analysis and more. In *Proceeding of the twelfth international conference on textures of materials (ICOTOM-12)*, 1999; NRC Research Press Ottawa, Canada: Vol. 1.
- [17] ISO, G. ISO/IEC GUIDE 98-3: 2008, Guide to the expression of uncertainty in measurement. *International Organisation for Standardisation, Geneva, Switzerland* **2008**.
- [18] Pirling, T.; Bruno, G.; Withers, P. J. SALSA—A new instrument for strain imaging in engineering materials and components. *Materials Science and Engineering: A* 2006, 437 (1), 139-144.
- [19] Konnecke, M., Akeroyd, F. A., Bernstein, H. J., Brewster, A. S., Campbell, S. I., Clausen, B., Cottrell, S., Hoffmann, J. U., Jemian, P. R., Mannicke, D., Osborn, R., Peterson, P. F., Richter, T., Suzuki, J., Watts, B., Wintersberger, E. & Wuttke, J. (2015). The NeXus data format. *J. Appl. Cryst.* 48, 301-305.
- [20] Richard, D.; Ferrand, M.; Kearley, G. Analysis and visualisation of neutron-scattering data. *Journal of Neutron Research* **1996**, 4 (1-4), 33-39.
- [21] Arnold, O.; Bilheux, J. C.; Borreguero, J. M.; Buts, A.; Campbell, S. I.; Chapon, L.; Doucet, M.; Draper, N.; Leal, R. F.; Gigg, M. A.; et al. Mantid-Data analysis and visualization package for neutron scattering and mu SR experiments. *Nucl Instrum Meth A* 2014, 764, 156-166. DOI: 10.1016/j.nima.2014.07.029.
- [22] Webster, P.; Mills, G.; Wang, X.; Kang, W.; Holden, T. Impediments to efficient through-surface strain scanning. *Journal of neutron research* 1996, 3 (4), 223-240.
- [23] Wang, X.-L.; Spooner, S.; Hubbard, C. Theory of the peak shift anomaly due to partial burial of the sampling volume in neutron diffraction residual stress measurements. *J Appl Crystallogr* 1998, 31 (1), 52-59.
- [24] Lorentzen, T. Numerical analysis of instrumental resolution effects on strain measurements by diffraction near surfaces and interfaces. *Journal of Neutron Research* 1997, 5 (3), 167-180.
- [25] Wang, X.-L.; Wang, Y.; Richardson, J. Experimental error caused by sample displacement in time-of-flight neutron diffractometry. *J Appl Crystallogr* 2002, 35 (5), 533-537.
- [26] Hutchings, M. T.; Withers, P. J.; Holden, T. M.; Lorentzen, T. *Introduction to the characterization of residual stress by neutron diffraction*; CRC press, 2005.
- [27] M. Gelfi, E. Bontempi, R. Roberti, L. E. Depero, X-ray diffraction Debye Ring Analysis for Stress measurement (DRAST): a new method to evaluate residual stresses, *Acta Materialia*, 52, 583 – 589 (2004).
- [28] Bob B. HE, Two-dimensional X-ray diffraction, John Wiley & Sons, Inc (2008). ISBN: 978-1-119-35608-0.
- [29] Hammersley, A. FIT2D: a multi-purpose data reduction, analysis and visualization program. *J Appl Crystallogr* **2016**, 49 (2), 646-652.
- [30] Apel, D.; Meixner, M.; Liehr, A.; Klaus, M.; Degener, S.; Wagener, G.; Franz, C.; Zinn, W.; Genzel, C.; Scholtes, B. Residual stress analysis of energy-dispersive diffraction data using a two-detector

setup: Part I—Theoretical concept. *Nuclear Instruments and Methods in Physics Research Section A: Accelerators, Spectrometers, Detectors and Associated Equipment* **2018**, 877, 24-33.

[31] <https://p61a-software.github.io/P61AToolkit/viewer/tut1.html>

[32] https://hdf5.gitlab-pages.esrf.fr/nexus/nxstress_examples/classes/contributed_definitions/NXstress.html

[33] Wimpory, R. C.; Ohms, C. A step towards a complete uncertainty analysis of residual stress determination using neutron diffraction. In *Materials Science Forum*, 2010; Trans Tech Publ: Vol. 638, pp 2487-2492.

[34] Pirling, T.; Hughes, D. J.; Robinson, J. S. Precise determination of residual stresses in large specimens by neutron diffraction. In *Materials Science Forum*, 2010; Trans Tech Publ: Vol. 652, pp 80-85.